OCO D-55009

OCO (Orbiting Carbon Observatory) - 2

Level 1B
Algorithm Theoretical Basis

Version 1.1 Rev 0
December 30, 2014

National Aeronautics and

Space Administration

JPL

Jet Propulsion Laboratory

California Institute of Technology

Pasadena, California

ORBITING CARBON OBSERVATORY (OCO) - 2

LEVEL 1B

Theoretical Basis Document

Prepared by:

Annmarie Eldering	Jet Propulsion Laboratory/ California Institute of Technology
Randy Pollock	Jet Propulsion Laboratory/ California Institute of Technology
Richard Lee	Jet Propulsion Laboratory/ California Institute of Technology
Robert Rosenberg	Jet Propulsion Laboratory/ California Institute of Technology
Fabiano Oyafuso	Jet Propulsion Laboratory/ California Institute of Technology
Robert Granat	Jet Propulsion Laboratory/ California Institute of Technology
David Crisp	Jet Propulsion Laboratory/ California Institute of Technology

Approved by: _____

Michael Gunson
OCO-2 Project Scientist
NASA Jet Propulsion Laboratory

Version 1.1
December 30, 2014

Jet Propulsion Laboratory
California Institute of Technology
Pasadena, California

Document History:

Version	Revision	Date	Description/Comments
1.0	0	April 14, 2014	Initial version of OCO-2 L1B ATBD
1.1	0	December 30, 2014	Updated in preparation for L1b public release.

The research described in this document was carried out at the Jet Propulsion Laboratory, California Institute of Technology, under a contract with the National Aeronautics and Space Administration.

TABLE OF CONTENTS

1. Scope of This Document and Background

The OCO-2 Data User's Guide discusses the OCO-2 mission objectives and measurements, including instrument characteristics. Please refer to that document for details of the data collection and naming convention. The focus of this algorithm theoretical basis document (ATBD) is to describe the Level 1B data and the process used to transform the inherent instrument measurements (L1A data) into radiometrically calibrated spectra (L1B data, Figure 1). The reader is encouraged to obtain details of the analyses of the instrument test data from published articles referenced in this document.

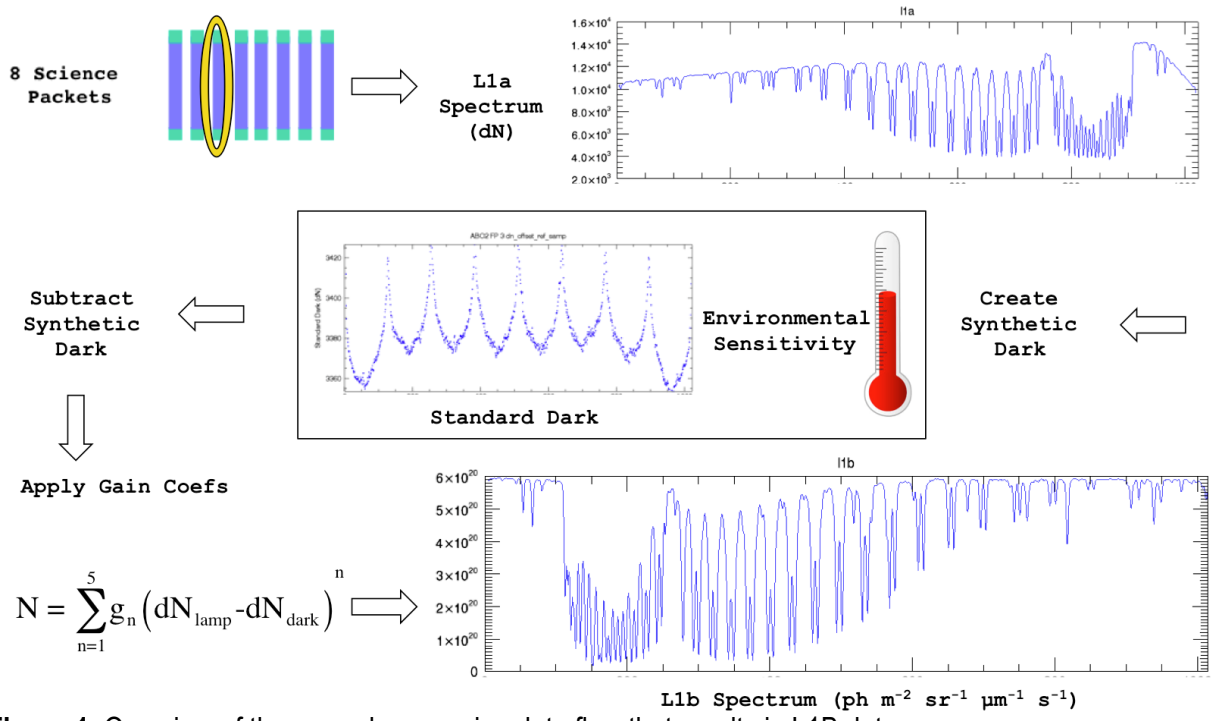

Figure 1. Overview of the ground processing data flow that results in L1B data.

1.1 Instrument Characteristics

1.1.1 Instrument Optical Path

The OCO-2 instrument incorporates three, co-boresighted, long-slit, imaging grating spectrometers optimized for the O_2 A-band at 0.765 microns (μm) and the CO_2 bands at 1.61 and 2.06 μm. The three spectrometers use similar optical designs and are integrated into a common structure to improve system rigidity and thermal stability. They share a common housing and a common F/1.8 Cassegrain telescope (Figure 1-1). Light entering the telescope is focused at a field stop and then re-collimated before entering a relay optics assembly. There, it is directed to one of the three spectrometers by dichroic beam splitters, and then transmitted through a narrowband pre-disperser filter. The pre-disperser filter for each spectral range transmits light with wavelengths within ~1% of the central wavelength of the CO_2 or O_2 band of interest and rejects the rest. The light is then refocused on the spectrometer slits by a reverse Newtonian telescope.

Each spectrometer slit is about 3 mm long and about 25 μm wide. These long, narrow slits are aligned to produce co-boresighted fields of view that are ~0.0001 radians wide by ~0.0146 radians long. Because the diffraction gratings efficiently disperse only the light that is polarized in the direction perpendicular to the long axis of the slit, a linear polarizer was included in front of the slit to reject the unwanted polarization before it enters the spectrometer, where it could contribute to the scattered light background. Once the light traverses a spectrometer slit, it is collimated by a 2-element refractive collimator, dispersed by a gold-coated, reflective, planar, holographic diffraction grating, and then focused by a 2-element camera lens onto a 2-dimensional focal plane array (FPA), after traversing a second, narrowband filter. The narrowband filter just above the FPA is cooled to ~180K to reject thermal emission from the

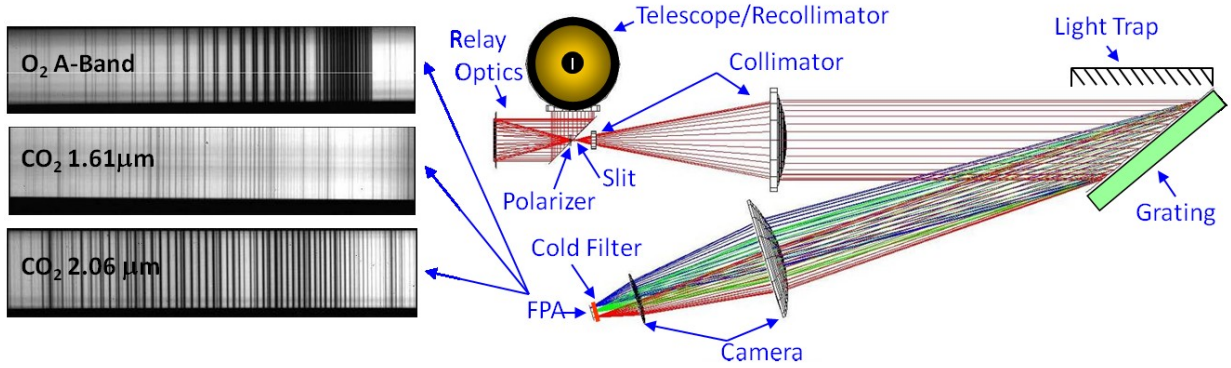

Figure 1-1. The OCO-2 instrument showing the major optical components and optical path (right) and images of spectra recorded by the FPA in the 3 spectral channels (left).

instrument.

An on-board calibrator (OBC) has been integrated into the telescope baffle assembly [Crisp et al. 2008]. This system consists of a calibration "propeller" that carries an aperture cover (lens cap) and a transmission diffuser. The cover is closed to protect the instrument aperture from external contamination during launch and orbit maintenance activities. It is also closed to acquire "dark frames" that are used to monitor the zero-level offset of the FPAs. The back side of the cover has a diffusively reflecting gold surface that can be illuminated by one of 3 tungsten lamps installed in the baffle assembly. The lamp "flat field" images are used to monitor the relative gain of the individual pixels on the FPAs. The calibration propeller is rotated 180 degrees from the closed position to place the transmission diffuser in front of the aperture to acquire observations of the sun. Routine observations of the sun are acquired just after the spacecraft crosses the northern terminator on all orbits except those that include downlinks. These measurements are used to monitor the absolute radiometric calibration of the instrument. The diffuser is also used to acquire solar spectra for full dayside orbits, which sample the full range of Doppler shifts (± ~7 km/sec) observed over the illuminated hemisphere. The calibration mechanism is rotated 90 degrees from either the closed or diffuser positions for normal science observations.

1.1.2 Focal Plane Array Detectors

The spectrometer optics produce a 2-dimensional image of a spectrum on a 1024 by 1024 pixel FPA with 18 μm pixels (Figures 1-2 and 1-3). The grating disperses the spectrum onto 1016 of the 1024 FPA columns (4 columns are blanked out on each side of the FPA) in the direction perpendicular to the long axis of the slit. The full-width at half maximum (FWHM) of the slit image on the FPA is sampled by 2 to 3 pixels in the direction of dispersion. The 3 mm long slit limits spatial field of view to only ~190 pixels in the dimension orthogonal to the direction of dispersion. Science measurements are restricted to the center ~160 of these 190 pixels.

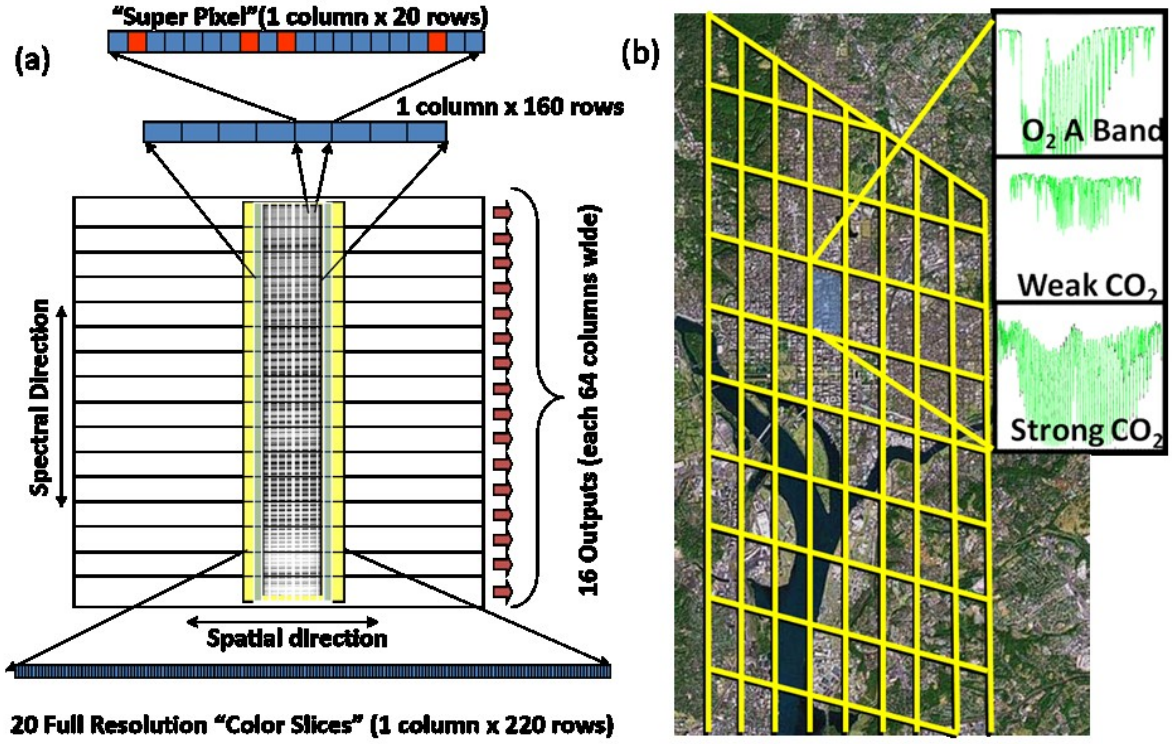

Figure 1-2. (a) The illumination and readout scheme used for the OCO-2 FPAs, showing the direction of spectral dispersion from bottom to top, and the spatial dimension from left to right. The ~160 illuminated pixels in the spatial dimension are summed into eight 20-pixel "super pixels" or "footprints." If one or more of the pixels in a footprint is "bad" (red pixels), it is eliminated from the sum. One of the 20 full-resolution "color slices" is also shown at the bottom. (b) Spatial layout of 8 cross-track footprints for nadir observations over Washington DC. Each footprint is shaped like a parallelogram, rather than a square, because of the rolling readout of the FPA's.

For normal science operations, the FPAs are continuously read out at 3 Hz. A "rolling readout" scheme has been adopted for reading out and resetting the FPAs, precluding the need for a physical shutter and gaps between the exposures. To reduce the downlink data volume and increase the signal to noise ratio, ~20 adjacent pixels in the FPA dimension parallel to the slit (i.e. The "Spatial Direction" in Figure 1-2a) are summed on board to produce up to 8 spatially-averaged spectra along the slit, to produce "spectral sample" for a "summed footprint."

The along-slit angular field of view of each of these spatially-averaged spectral samples is ~1.8 milliradians (0.1° or ~1.3 km at nadir from a 705 km orbit). The angular width of the narrow

dimension of the slit is only 0.14 milliradians, but the focus of the entrance telescope was purposely blurred to increase the effective full width at half maximum of each slit to ~0.6 milliradians to simplify the bore-sight alignment among the 3 spectrometer slits. Because it takes 0.333 seconds to can across the active, 220-rows of the array, the surface footprints of the 8 spatially averaged spectra are read out at 0.03 second intervals, and are shaped liked parallelograms, rather than squares, even when the slit is oriented orthogonal to the ground track (Figure 1-2b).

In addition to the 8 spatially-binned, 1016-element spectra, each spectrometer returns up to 20 columns from each FPA without any on-board spatial binning to sample the full along-slit spatial resolution. Each of these full-resolution "color slices" images a 220-pixel wide region of the FPA that includes the full length of the slit (~190 pixels) as well as a few pixels beyond the ends of the slit (Figure 1-2a). These full-spatial-resolution "color slices" are used to detect spatial variability within each of the spatially summed super pixels and to quantify the thermal emission and scattered light within the instrument. Their locations can be specified by commands from the ground.

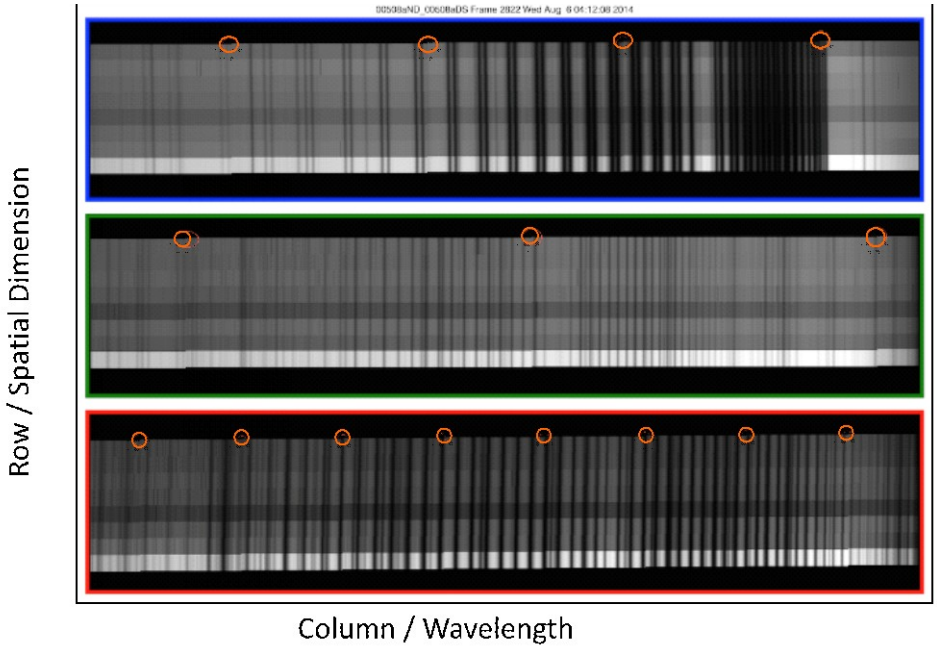

Figure 1-3. Images of the O2 A-Band (top), 1.61 □m CO2 band (middle) and the 2.06 □m CO2 band (bottom) in "summed mode" taken from the OCO-2 first light frame over Papua New Guinea. The 8, spatially-summed footprints in each band are shown from bottom (footprint 1) to top (footprint 8). In this 0.333 second frame, footprint 1 was contaminated by a cloud and appears brighter than the rest. This frame clearly shows the rotation, or "clocking" of each FPA columns with respect to the dark O2 and CO2 absorption lines. The O2 lines are tilted slightly counterclockwise, while the 1.61 and 2.06 □m lines are tilted clockwise. The columns where the clocking corrections are applied are highlighted with red circles. Soundings collected in regions with strong spatial gradients in illumination can produce radiance discontinuities at these wavelengths.

In this instrument design, the spectrometer slits, the grooves on the diffraction gratings, and columns of the FPAs must be well aligned to ensure that a fixed series of rows on the FPA will sample the same angular field of view (or spatial footprint) throughout the spectral range recorded by the FPA. For the OCO-2 instrument, perfect alignment of the FPAs with the other optical components was not possible due to a physical obstruction discovered late in the instrument assembly process. The focal plane arrays are therefore slightly rotated (or "clocked") with respect to the slit and grating. Consequently, a given geographic position does not map onto a single row of pixels on a sensor, but instead varies (roughly linearly) with spectral position (i.e. column). To compensate for this, and record the same spatial information across the entire spectrum, the starting row index for each spectral sample can be adjusted in increments of one pixel. This corresponds to about 1/20th of a summed footprint (Figure 1-3). This approach introduces little error in spatially homogenous scenes, but can produce discontinuities in spectra of scenes with strong intensity variations near the edge of a footprint. These discontinuities will eventually corrected as part of the calibration process (see the Level 1B Algorithm Theoretical Basis Document).

1.1.3 Bad Pixels and Bad Samples

OCO-2 is flying flight-spare FPAs from the OCO mission, which were delivered in 2006. A small fraction of the 220,000 pixels in the active area of these arrays are either dead, or respond to light or thermal changes is a way that is not consistent with the majority of the other pixels. These pixels must be identified and excluded from the 20-pixel sums that are performed onboard, or they will contaminate the resulting 20-pixel "spectral samples" that constitute the spectra returned for the 8 footprints by each spectrometer. Spectral samples with too many bad pixels, or with other known issues (e.g. optical artifacts on the short-wavelength ends of all 3 bands) are marked as bad in the Level 1B product, so that they are not used in producing higher level products.

The bad pixel identification process was started during pre-launch testing, but must be updated on orbit because additional pixels have degraded during the 2.5 year instrument storage period prior to launch, and others are damaged on-orbit by cosmic radiation and other effects. To identify bad pixels, the calibration team routinely collects dark and lamp data using "single pixel" mode, which returns all 220,000 pixels in the active region of each array. (Single-pixel results cannot be returned routinely for science observations because it requires ~9 second to read out an FPA at full resolution.) These single-pixel data are then analyzed to identify bad pixels and add them to a "bad pixel map" that is uploaded to the spacecraft for use in the pixel-summing process. As the bad pixel maps improve, a larger faction of the spectral samples in each spectrum can be used to generate Level 2 products.

1.1.4 Cosmic Ray Artifacts

Cosmic rays rarely produce permanent damage to the OCO-2 FPAs, but this radiation produces ion trails as they traverse the FPAs, producing spurious intensity spikes. Primary and secondary cosmic rays with a broad range of energies are occasionally seen just about anywhere along the

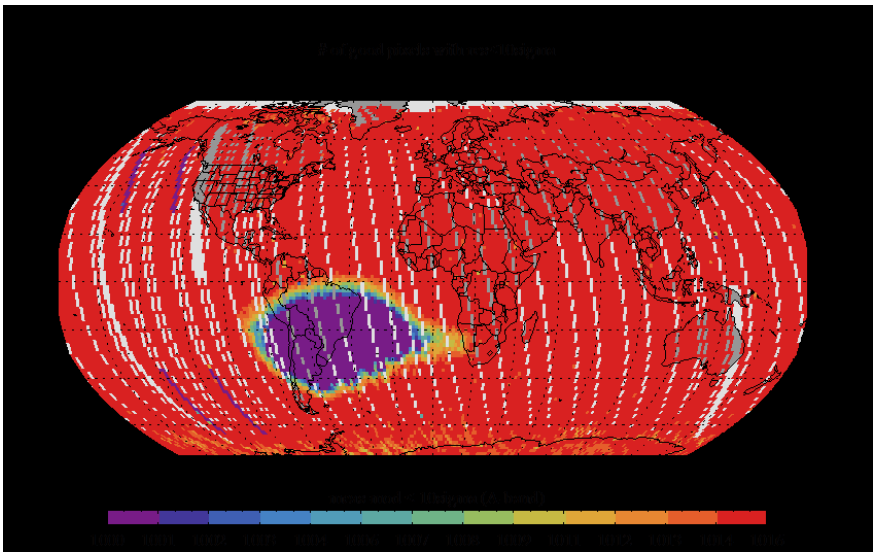

Figure 1-4: The number of spectral samples in the O2 A-band that are not contaminated by 10-signma cosmic rays events clearly shows the geographical extent of the South Atlantic Anomaly (SAA).

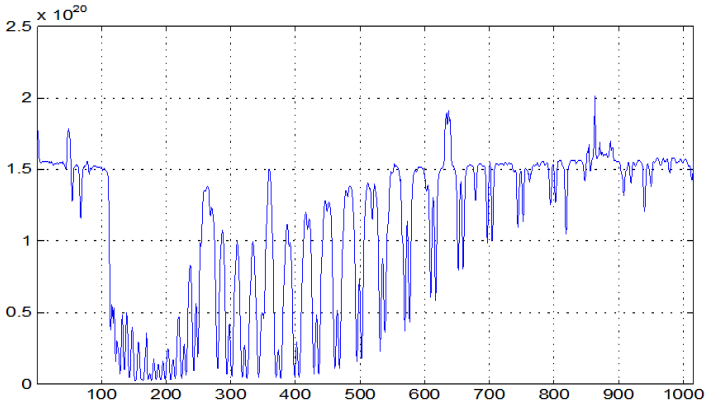

Figure 1-5 An example showing the impact of a radiation event on spectra. Note the three spikes with unusually high intensities.

orbit path but they are most common in the vicinity of the South Atlantic Anomaly (SAA), where up to 2% of an O_2 A-band spectral range can be contaminated in individual spectra. The approximate geographical extent of the SAA as it impacts the OCO-2 mission can be seen in Figure 1-5. An algorithm has been developed to identify and screen cosmic rays, but was not implemented in time for the initial Level 1B data release. These artifacts will be identified in future releases.

1.2 Radiometric Overview

The focal planes are read out in unitless data numbers (dNs), and these are referred to as the L1A Spectrum (see Figure 1). The first data processing step is to apply dark correction. During thermal vacuum testing, a set of data was collected with the light source shuttered such that no light entered the instrument. This dark data is used to characterize the response of the focal planes with no illumination. As discussed in Rosenberg et al. [2014], this is important because a dN offset can introduce a linearity error. During orbit, dark data will be collected and the dark subtraction will be updated early in the mission. The dark data will be monitored thereafter and updated if needed.

The next step is to apply gain curves, which describe the relationship between dN and calibrated radiance. The preflight gain curves are described in more detail in Rosenberg et al. [2014]. The sections below describe the approach for in-flight updates.

1.3 Spectral Response Overview

To properly use the L1B data, the instrument line shapes (ILS) must be determined. These are contained in the L1BSc files in two key fields: ils_delta_lambda and ils_relative_response. ILS are covered in more detail below, and their use is described in the Data User's Guide.

Dispersion coefficients are also provided in the L1BSc files (dispersion_coef_samp) to convert the focal plane sample pixel index to a wavelength scale. In the L2 retrieval of geophysical quantities, the Doppler shift is accounted for and the dispersion is corrected for each sounding.

1.4 In-Flight Measurements

In flight, three radiometric calibration measurements are routinely collected: solar calibration, dark calibration, and vicarious calibration data.

For solar calibration, the Observatory views the Sun through the diffuser just before eclipse, holding a steady viewing angle to observe atmospheric spectra at various optical depths unaffected by significant pressure broadening or surface reflection. These measurements are used to verify the spectral response of the spectrometer.

For dark calibration, the Observatory collects data with the aperture door closed and the lamps off. This calibration is repeated at various eclipse-side latitudes.

In addition to these routine calibrations, two types of special calibrations are performed. The first is Solar Doppler calibration, where the solar diffuser is placed over the telescope aperture, and solar observations are collected over a full dayside orbit, sampling the full range of Doppler shifts observed as the spacecraft travels $\pm$ 7 km/sec toward and away from the sun. These measurements provide very high resolution solar radiometric observations, and are also used to monitor the instrument line shape (ILS).

The second type of special observation is

For vicarious calibration, the Observatory targets Railroad Valley, Nevada, a ground site with a well-characterized surface, where there is sufficient instrumentation to make absolute radiance measurements. More details can be found in Kuze et al. [2011; 2013].

2. Radiometry

2.1 Bad Pixel Map

The bad pixel map is a 1024x220x3 byte array where a value of 1 indicates that a pixel's signal should not be used. Bad pixels are corrected by the flight computer in space, as part of producing sample mode ("summed") data. The single pixel readings are never returned to the ground during nominal science operations. Within each column, a single or double bad pixel is replaced by the average of the closest neighboring good pixels on each side. If three or more bad pixels exist within a column, those values are set to 0. As a result, a pixel can have a weight of 0, 1, 1.5, 2, 2.5, or 3 in the nominal 20 pixels that constitute a sample. Many sample mode calibration fields (gain, noise model, dark correction coefficients) needed to be updated with each bad pixel map change to reflect the new weighting.

2.1.1 Bad Pixel Map Usage

The bad pixel map is used only in SUMMED and RESIDUAL modes. The bad pixel map does not apply to single pixel mode. The bad pixel map also does not apply to the color slices downlinked in the optical housekeeping packets.

2.1.2 Summed Mode Pixel Map Processing

All identified bad pixels are mitigated before the instrument software applies any pixel summation algorithms.

2.1.3 Bad Pixel Map / Footprint Relationship

The OCO-2 instrument digitizes an array 220 spatial pixels by 1024 spectral pixels. Summed science data uses the "middle" 160 spatial pixels. The "middle" 160 pixels correspond to rows 30 thru 189 (160 rows). This relationship is shown in Figure 2.

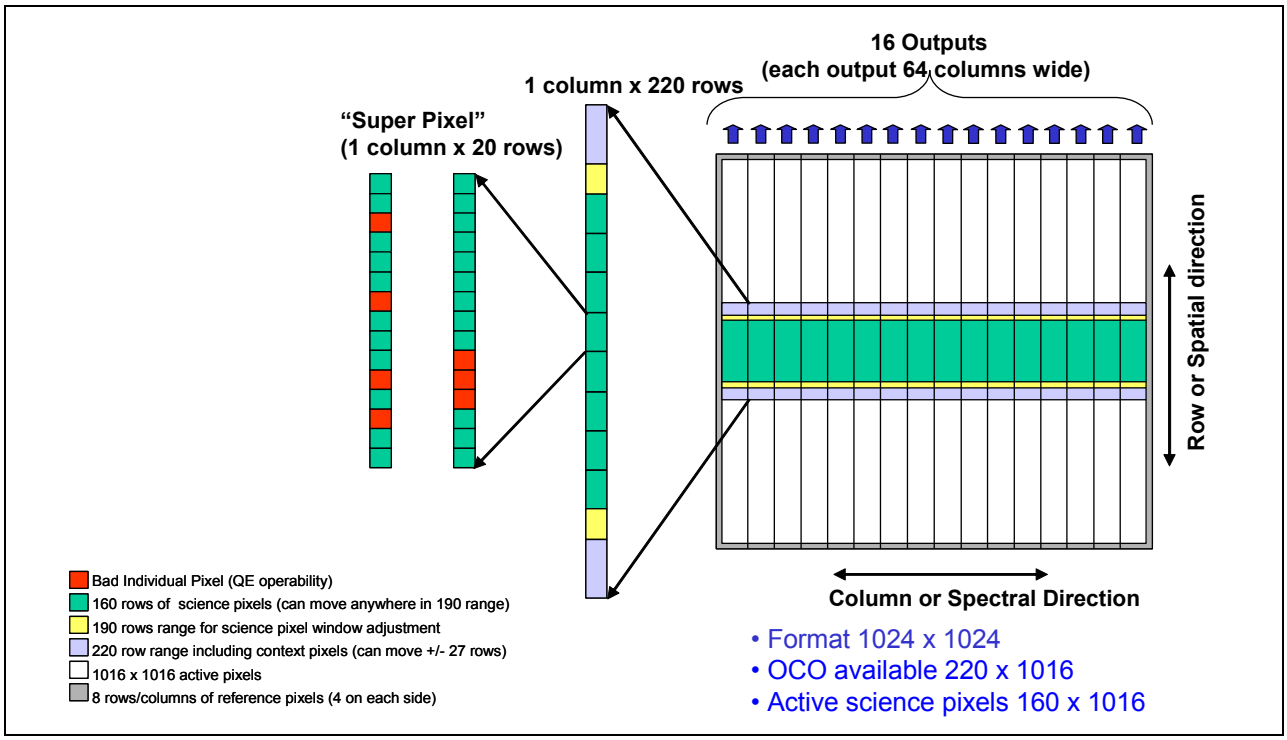

Figure 2 – Focal Plane Readout Definition

For example, with eight footprints each twenty pixels wide, the corresponding footprint limits are shown in Table 1.

Table 1 – Example Footprint Limits

Footprint	Limits
1	30 – 49
2	50 – 69
3	70 – 89
4	90 – 109
5	110 – 129
6	130 – 149
7	150 – 169
8	170 - 189

The pixel map is always referenced to the 220 x 1024 digitized array. Thus, using the example, the smallest pixel map row value should be 30. For the example shown, the largest pixel map row value should be 189. In order to be most useful, the pixel map limits should correspond to the limits defined in the footprint start and end limits.

Pixel mitigation is performed without regard to footprint limits or boundaries. Pixel mitigation is not impacted by masked or unmasked footprints. It is up to the user to make sure that only deserving pixels are mitigated.

2.1.4 Bad Pixel Mitigation Calculations

Bad pixels are mitigated as shown in Table 2. Bad pixel mitigation is only performed in the spatial direction in the digitized array. There is no correction performed in the spectral direction.

Table 2 – Bad Pixel Mitigation

Bad Pixel Configuration	Mitigation
Single bad pixel	Replaced with the average of the two spatially adjacent good pixel values
Double bad pixel	Replaced with the average of the two spatially adjacent good pixel values. The same values is used to replace both bad pixel values
Triple bad pixel	All bad pixels are replaced with zero values

2.2 Dark Subtraction

Temperature variations of the optics and FPAs contribute to the dark background signal. The as-measured dN values can be corrected for these effects using the dark subtraction equation:

$$dn_{corrected} = \left(dn_{raw} - dn_{ref}\right) + c_{optics}\left(T_{optics}(t) - T_{ref\_optics}\right) + c_{FPA}\left(T_{FPA}(t) - T_{ref\_FPA}\right)$$

where

- $dn_{corrected}$ —dN after dark correction
- dn_{raw} —as-measured dN
- dn_{ref} —dN detected with no illumination
- c_{optics} —optics temperature dependence coefficients
- $T_{optics}(t)$ —optics temperature as a function of time (in L1B data product as FrameTemperatures/temp_smooth_optical_bench_grating_mz)
- T_{ref_optics} —the optics temperature that will yield dn_{ref}
- c_{FPA} —FPA temperature dependence coefficients
- $T_{FPA}(t)$ —O_2, weak CO_2, and strong CO_2 FPA temperatures as a function of time (in L1B data product as FrameTemperatures/temp_smooth_fpa_[o2, weak_co2, strong_co2])
- T_{ref_FPA} —the O_2, weak CO_2, and strong CO_2 FPA temperatures that will yield dn_{ref}

dn_{raw}, dn_{ref}, c_{optics}, and c_{FPA} have dimensions of 1024 x 8 x 3—a value for each column, footprint, and band. These are in the Ancillary Radiometric Product (ARP) but are not provided in the L1B files.

Dark current in the OCO-2 detectors is partially dependent on different voltages and temperatures within the instrument. To minimize science impact, dark correction performed in the conversion from L1A to L1B includes simultaneous adjustments for two temperatures. To avoid introducing errors due to noise in the temperature sensors, temperatures are smoothed before they are used. Note that all temperatures except for the FPA temperatures are only updated every 15 seconds. Temperatures are smoothed over an entire orbit using a linear fit, performed before the orbit is broken into several files at mode change boundaries.

2.3 Radiometric Gain

Because atmospheric absorption is inferred from the ratio between continuum and line core radiances, the radiometric calibration must account for any nonlinearities in the instrument gain. Even though the instrument gain appears near linear, it is described using a 5th order polynomial of radiance vs. signal to describe any nonlinear effects:

$$Radiance = k \sum_{i=0}^{5} c_i \left(dn_{dark\_corrected} \right)^i$$

The k terms, referred to as gain_degrad_samp, (k) will be set to 1.0 at launch. The gain_degrad_samp term in-flight will be determined through the vicarious calibration experiments that were mentioned earlier.

The c_i terms are referred to as gain_preflight_samp, (c_i). At launch, these are set based on a combination of the best five radiometric calibration tests during final instrument testing at JPL. While the algorithm allows an offset term ($i = 0$), the c_0s are all set to zero as dark subtraction is

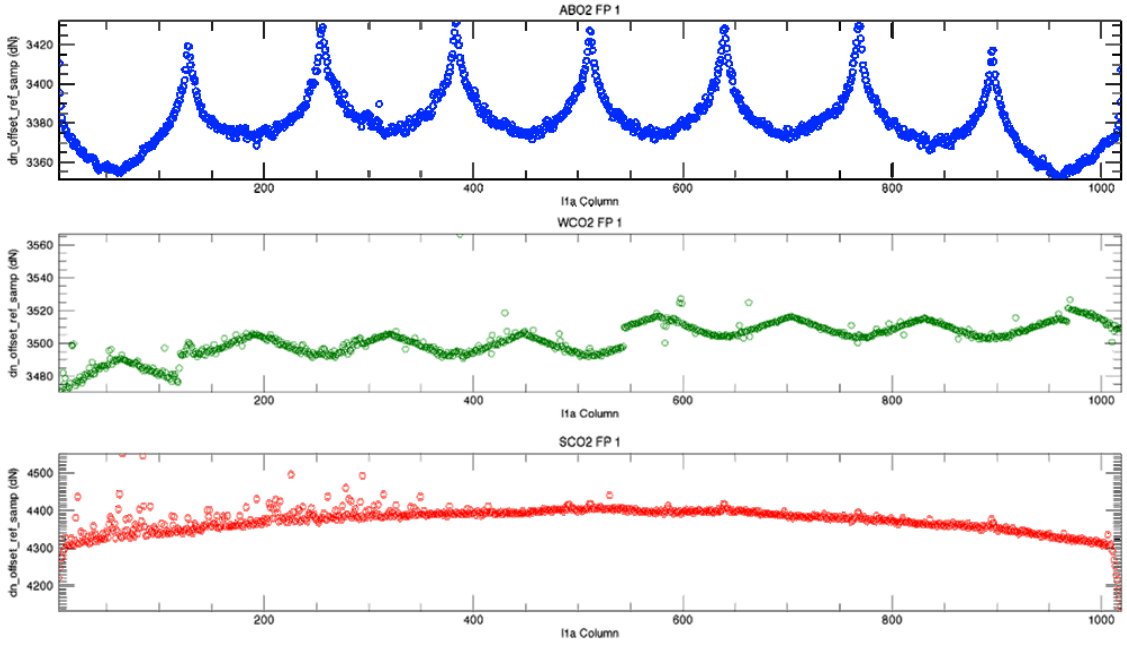

Figure 3. Example of a term in the dark subtraction (dn_{raw}).

made in the earlier computational step. No significant improvement was observed after cubic correction, so the c_4s and c_5s are also set to zero. The determination of the gain_preflight_samp coefficients is described in detail in Rosenberg et al. [2014]. These values will not change on-orbit except in samples with newly-flagged bad pixels.

An example of the application of this equation (for the strong CO_2 band, column 500, footprint 3) is:

$$\text{Radiance} = 0 + 2.898 \text{ x } 10^{15} \cdot \text{dn} + 1.902 \text{ x } 10^{9} \cdot \text{dn}^2 + 9.559 \text{ x } 10^{3} \cdot \text{dn}^3 + 0 \cdot \text{dn}^4 + 0 \cdot \text{dn}^5$$

3. Signal-to-Noise Ratio

3.1 Calculation of SNR

The noise values are not stored directly in the file, but they can be calculated using a few fields in the L1bSc data file and the following formulas for the noise equivalent radiance and consequently the SNR:

$$NEN = \frac{MaxMS}{100} \cdot \sqrt{\left|\frac{100 \cdot N}{MaxMS}\right| \cdot C_{photon}^2 + C_{background}^2}$$

$$SNR = \sqrt{\frac{100\,N^2}{MaxMS * \left(C_{background}^2 \frac{MaxMS}{100} + C_{photon}^2 N\right)}}$$

where

- N —radiance value
- $MaxMS$ —maximum measurable signal per band (see below)
- C_{photon} —first coefficient of L1bSc/InstrumentHeader/snr_coef ([0, *, *, *])
- $C_{background}$ —second coefficient of L1bSc/InstrumentHeader/snr_coef ([1, *, *, *])

The third entry of L1bSc/InstrumentHeader/snr_coef (zero-based indices [2, *, *, *]) is used to identify bad samples that should be excluded by the retrieval algorithms. The third entry can range between 0 and 15 and is the sum of the following byte codes:

0 = Good
1 = Radiometric Problem (e.g. jumping pixel that needs to be identified for future bad pixel map, linearity problems)
2 = Spatial Problem (e.g. low wavelength 100 columns)
4 = Spectral Problem (e.g. ILS not trustworthy - last couple of samples on the CO2 bands where the mask shadows the FPA)
8 = Polarization Problem (no examples yet).

Figure 5 shows an example set of coefficients.

The *MaxMS* values are given in Table 3 below. The strong CO2 value was increased by 50% from OCO, and all values were halved to account for only one polarization being selected.

Table 3. *MaxMS* values.

Band	MaxMS value (photons/m^2/sr/µm)
O_2 A-band	$7.00*10^{20}$
Weak CO_2	$2.45*10^{20}$
Strong CO_2	$1.25*10^{20}$

3.2 Development of SNR Coefficients

The initial snr_coef are based on a combination of the data from the best five radiometric calibration tests during final instrument testing at JPL. While this model assumes a perfectly

linear detector, which is not the case, it still fits the data reasonably well. The only significant

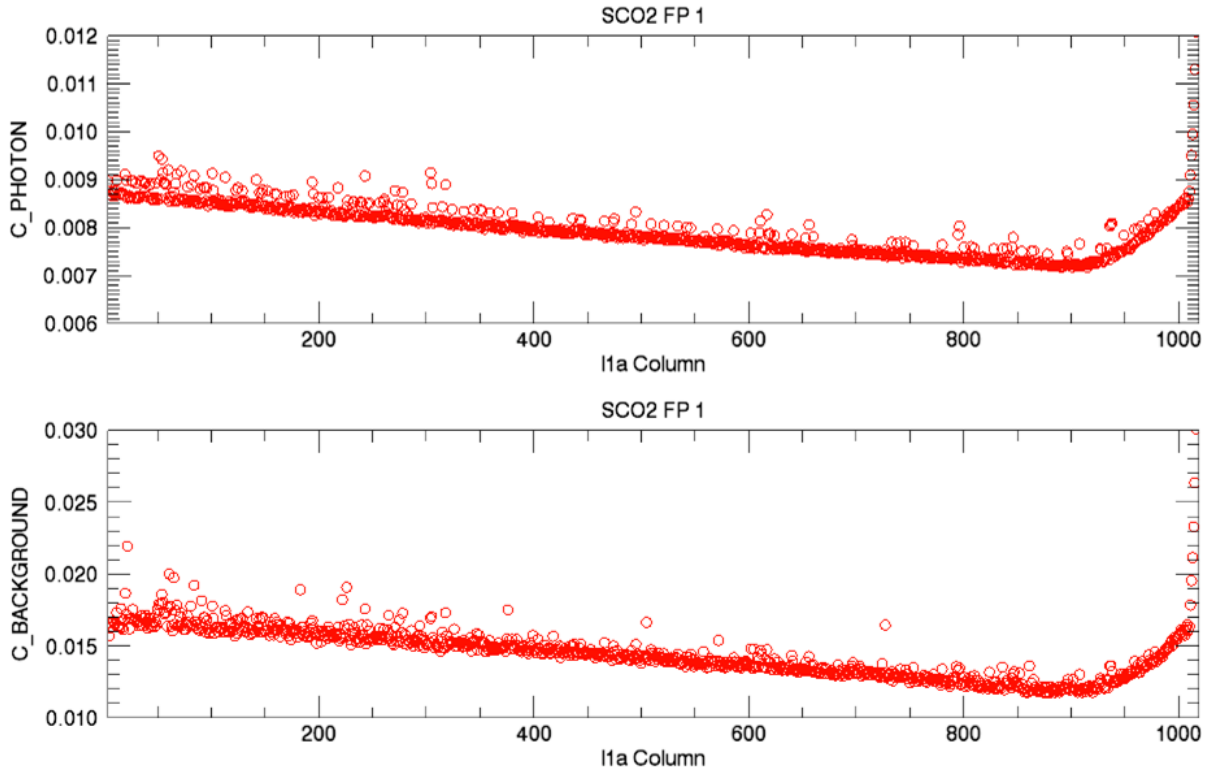

Figure 4. Example of signal-to-noise coefficients.

errors observed are at extremely low signal levels, where this SNR expression overestimates the radiance uncertainty because we do not currently include a term for uncertainty due to dark subtraction. The importance of this term will be further investigated in flight.

3.3 In-Flight Updates of SNR Coefficients

The dark noise (background term) will be updated based on the dark calibration data, measured directly during dark calibration periods (~12 two-minute dark calibration data collections each day).

Photon noise is assessed using solar calibration and lamp calibration data (our only consistent radiance scenes). We assume that the photon noise changes if the gain_degrad_samp term changes and adjust accordingly.

Later in the mission, a further assessment of the photon noise will be conducted by analyzing any changes in the residuals (differences between observed and calculated spectra determined in the L2 retrieval stage) for scenes that appear to have consistent radiances and retrieved state.

4. Spectral Response

4.1 Spectral Dispersion Coefficients

The dispersion coefficients express the relationship between the spectral element index (an individual pixel) and its associated wavelength (see Figure 5). These data are contained in L1bSc/InstrumentHeader/dispersion_coef_samp. Note that this grid does not account for the Doppler correction or dispersion adjustments that are applied in the L2 retrieval stage. The coefficients are used as follows:

$$\lambda = \sum_{i=0}^{5} c_i \,.\, \text{column}^i$$

where column refers to the column number in the L1bSc files (1 to 1016), which is raised to the power *i*.

An example calculation of the wavelength grid is:

$$\lambda = 0.757633 + 1.75265 \times 10^{-5} \cdot \text{column}^1 - 2.91788 \times 10^{-9} \cdot \text{column}^2 + 3.29430 \times 10^{-13} \cdot \text{column}^3 - 2.72386 \times 10^{-16} \cdot \text{column}^4 + 7.66707 \times 10^{-20} \cdot \text{column}^5$$

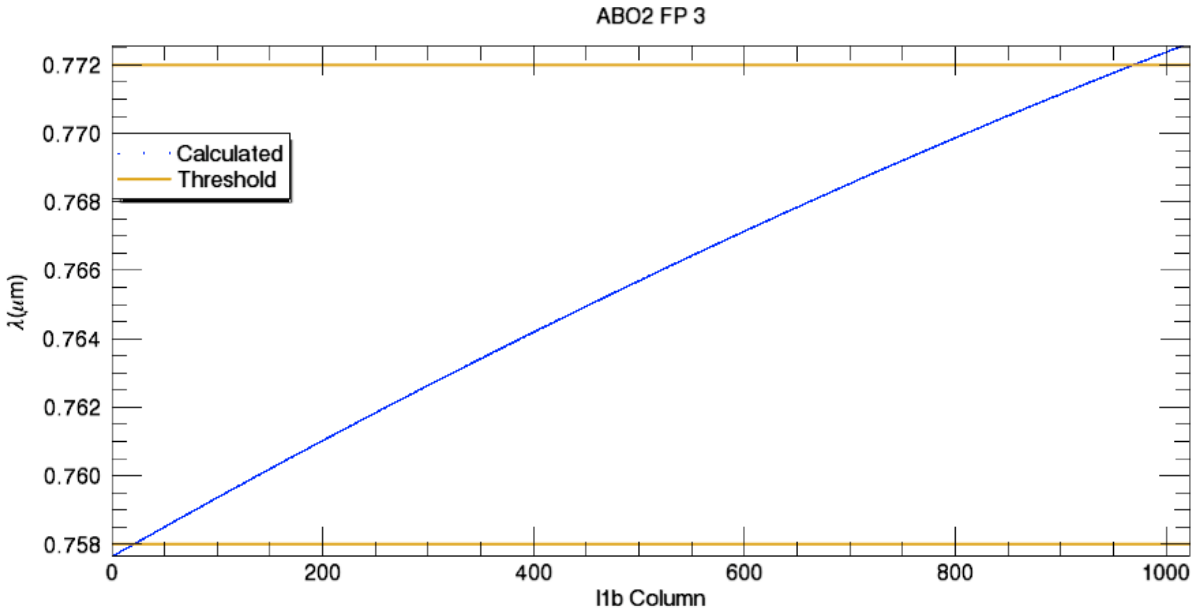

Figure 5. An example of the conversion of the focal plane column to wavelength scale. The blue line shows the column number-to-wavelength transformation. The yellow lines indicate the required wavelength range for this band.

4.2 Instrument Line Shape

The central challenge of the OCO-2 spectral calibration is determining not just a single ILS, but rather the ILS for each and every spectral pixel index, footprint, and band. The three bands, eight footprints per band, and 1016 spectral samples per footprint yield in theory 24,384 individual ILS functions. This is in contrast to, e.g., the Thermal and Near Infrared Sensor for Carbon Observations-Fourier transform spectrometer (FTS) aboard the Greenhouse Gases Observing Satellite (GOSAT), which in theory has just two ILS functions (one per polarization), as described by Yoshida et al. [2012]. However, the physics of the OCO-2 instrument design dictates that the ILS and centroid wavelength response (dispersion) of OCO-2 should vary smoothly in the spectral dimension across each band. The details of the measurements and analysis for determining the ILS are reported in Lee et al. [2015].

In the data product, for each band, footprint, and spectral element (3 x 8 x 1016 pixels), there are two 200-element lookup tables: L1bSc/InstrumentHeader/ils_delta_lambda and L1bSc/InstrumentHeader/ils_relative_response. These curves describe the response of each spectral element of the instrument versus wavelength, and can be used to convolve high spectral resolution spectra for comparison with OCO-2 spectra.

Initial determination of the ILS was performed using tunable diode lasers that were stepped through a range of wavelengths covering the OCO-2 spectral range. The final ILS was then optimized and validated by comparing solar spectra recorded simultaneously by OCO-2 and an FTS, as described by O'Dell et al. [2011]. As reported in Lee et al. [2015], the resulting ILS profiles (Figure 6) showed agreement between the two spectra to approximately 0.2% rms, satisfying the preflight calibration requirement of < 0.25% rms.

At the start of the mission, ils_delta_lambda and ils_relative_response were based on several laser and heliostat-based tests at JPL. At the start of the mission, ils_delta_lambda and ils_relative_response were based on several laser and heliostat-based tests at JPL Spectral residuals created during the retrieval stage using on-orbit data have been carefully analyzed for evidence of ILS errors. In the long term, the solar calibration mode provides an opportunity to look at relative changes in the ILS due to Doppler shifts. However, since the flight diffuser may make subtle changes the ILS, an absolute measurement may not be possible. As of December 2014, on-orbit examination of the spectral residuals indicates a stable ILS.

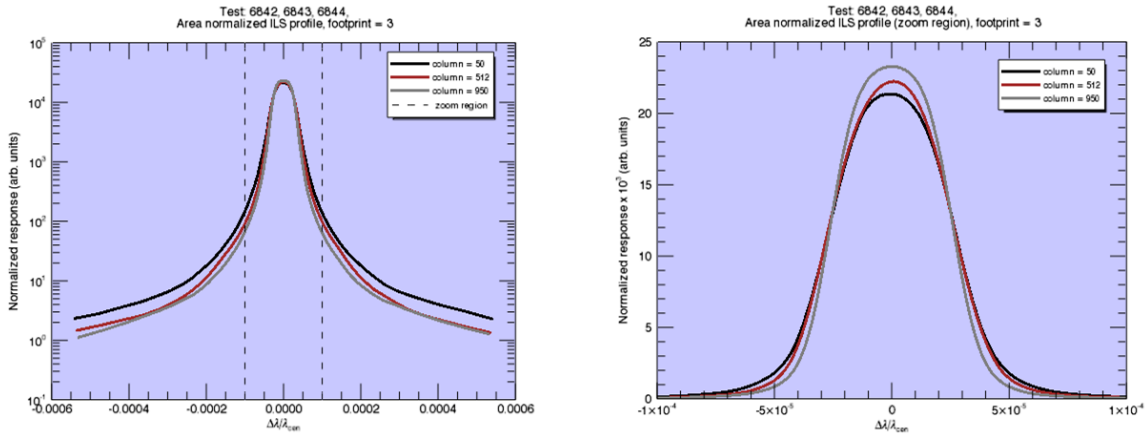

Figure 6. Example ILS profiles for the O_2 A-band at three different spectral pixel indexes. (Left) Semi-log plot of the ILS.(Right)Linear plot of the ILS core.

4.3 Clocking Correction

As noted in Section 1, in this instrument design, the spectrometer slits, the grooves on the diffraction gratings, and columns of the FPA's must be well aligned to ensure that a fixed series of rows on the FPA will sample the same spatial footprint throughout the spectral range recorded by each FPA. For the OCO-2 instrument, perfect alignment of the FPA's was not possible due to a physical obstruction discovered late in the instrument assembly process. The focal plane arrays are therefore slightly rotated (or "clocked") with respect to the slit and grating. Consequently, a given geographic position does not map onto a single row of pixels across the entire spectral range sampled by the FPA. Instead, it changes from row to (roughly linearly) with spectral position (i.e. column). This is not an issue in spatially homogeneous regions, but can introduce spectral radiance discontinuities for scenes with substantial variations in illumination across a given spatial sample. Identifying and correcting these discontinuities is complicated, somewhat, but the fact that instrument sums ~20 spatial pixels into each spectral sample that is transmitted to the ground. For example, in lunar calibration data, where radiances can fall from a maximal value to the noise level over a span of four or five pixels and where there are no obscuring absorption features, discontinuities are clearly discernable in nearly every measurement that is at least several times above the noise level. Methods for identifying and correcting these discontinuities are described in the following section.

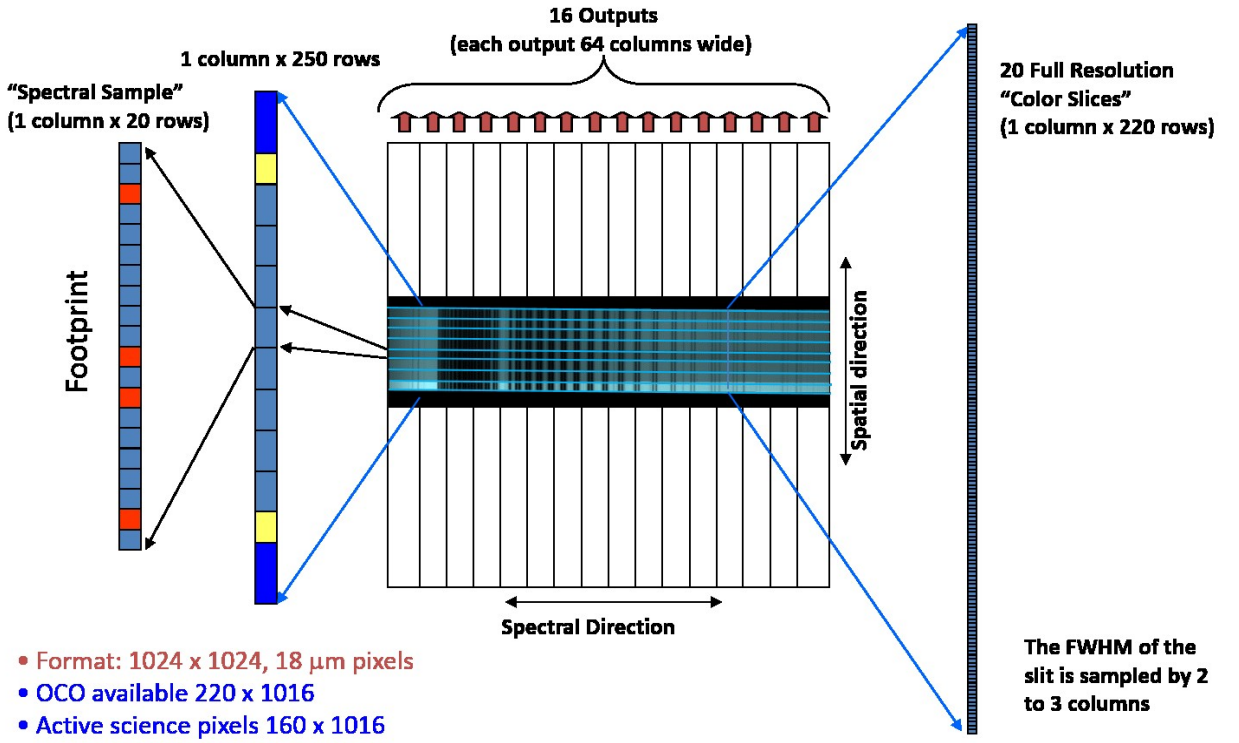

Figure 7: The illumination and readout scheme used for the OCO-2 FPA's. In this figure, the slit extends vertically, and the spectrum is dispersed from left to right.

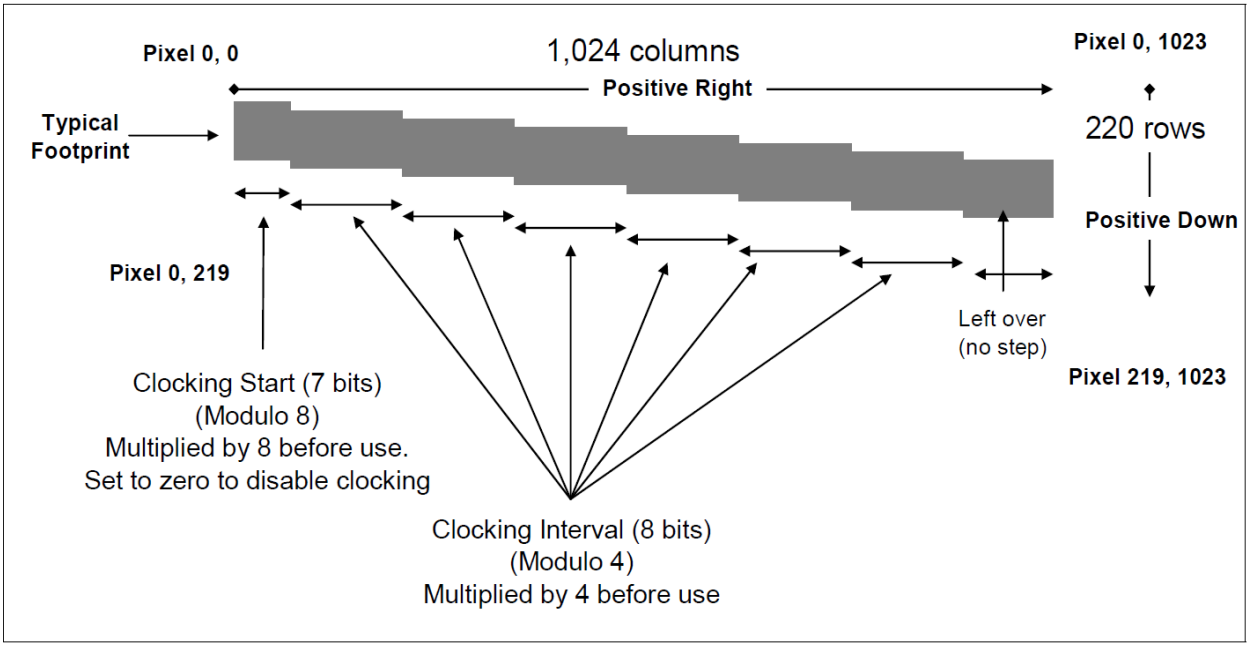

Figure 8: The "clocking" scheme used to sample the same spatial information (vertical dimension) across the entire spectral range (horizontal) for a rotated FPA.

Because fields of view must ultimately be mapped onto discrete pixels, the start and end positions of each footprint are adjusted in single pixel increments (i.e *clocking jumps*) in row space at selected columns (Fig. 3). These jumps can introduce discontinuities in the mean measured radiances for a spatial footprint if there are sharp gradients in the illumination near its boundaries. To compensate for these discontinuities, we have developed a simple clocking correction algorithm that enforces continuity in radiance across single pixel footprint shifts. The principal idea behind the algorithm is that although we do not have access to the full matrix of radiances over all rows and columns, we can use the entire row (i.e. spatial) information of some subset of the twenty color slices as a proxy for the spatial variation of intermediate columns, particularly those columns where clocking jumps occur. More specifically, at a small number of color slice positions we compute what the magnitude of the discontinuity in radiance would be if the slice position coincided with a particular clocking jump. We then make the assumption that this discontinuity is a valid approximation over some spectral neighborhood of the color slice and that the results from all the color slices can then be smoothly joined in some way.

The selection of which columns comprise the set of color slices can be altered by ground commands. One could place color slices adjacent to the columns with the clocking jumps. However, this is problematic for this application because some of these columns include sharp atmospheric or solar absorption features, and these features can be shifted by 2-3 columns by Doppler shifts associated with the spacecraft motion. If a color slice is placed in a region where the radiance changes rapidly (e.g. near an absorption line), the variation of radiance along a given row may be more indicative of the local spectral structure than of the spatial features of the measurement. Therefore, it is very important to place color slices where spectral variation is limited, i.e. in continuum regions. The availability of pixels in clear continuum regions varies substantially from band to band. For the O_2 A band (O2A), continuum regions were selected just beyond the measurable high J value lines of the P and R branches as well as between the two branches. A similar approach was adopted for the weak CO_2 band near 1.61 μm (WCO2). In contrast, the deeply saturated strong CO_2 band near 2.06 μm (SCO2) offers no spectral regions as transparent as

in the other two bands, and none of the color slices used by the clocking algorithm lies in between the P and R branches.

The figures on the following pages illustrate the nature of the clocking error and the choices of color slices for each of the three OCO-2 bands. For each band, there is a large figure which contains three different graphic elements. First are the nearly horizontal solid lines which delineate the boundaries of the eight footprints. The discrete jumps in the footprint boundaries illustrate the clocking effect. Note that the magnitude of the clocking effect varies among the bands, ranging from 8 discontinuities in the most severe case (SCO2) to 2 in the least (WCO2). Second, the dashed vertical lines indicate the current selection of all twenty color slices (as of October 2014). *Only those slices that are labeled by an index are used by the clocking algorithm.* Finally, a representative spectrum is superimposed to provide some context for the color slice selection.

Generally, the color slices used by the clocking algorithm are located in spectral regions with little absorption. Not all twenty color slices are used for clocking; other color slices have been located within strong absorbtion features to assess the spatial inhomogeneity due to clouds and aerosols or to monitor solar lines. In the O2A band, slices 16, 17, and 18 lie in the neighborhood of a solar line and were mistakenly included in the clocking correction. However, it was found that corrections using these slices correlate very strongly with those using slices 15 and 19, which do lie in the continuum, so that the inclusion of these color slices in the clocking correction algorithm is unlikely to have significant impact. Nevertheless, future versions of the clocking algorithm may remove these slices from consideration. Slices 3, 4, 5, and 15 from the SCO2 band may in the future be eliminated or replaced, since they lie close to weak absorption lines. Further testing is required to determine what difference their omission would make.

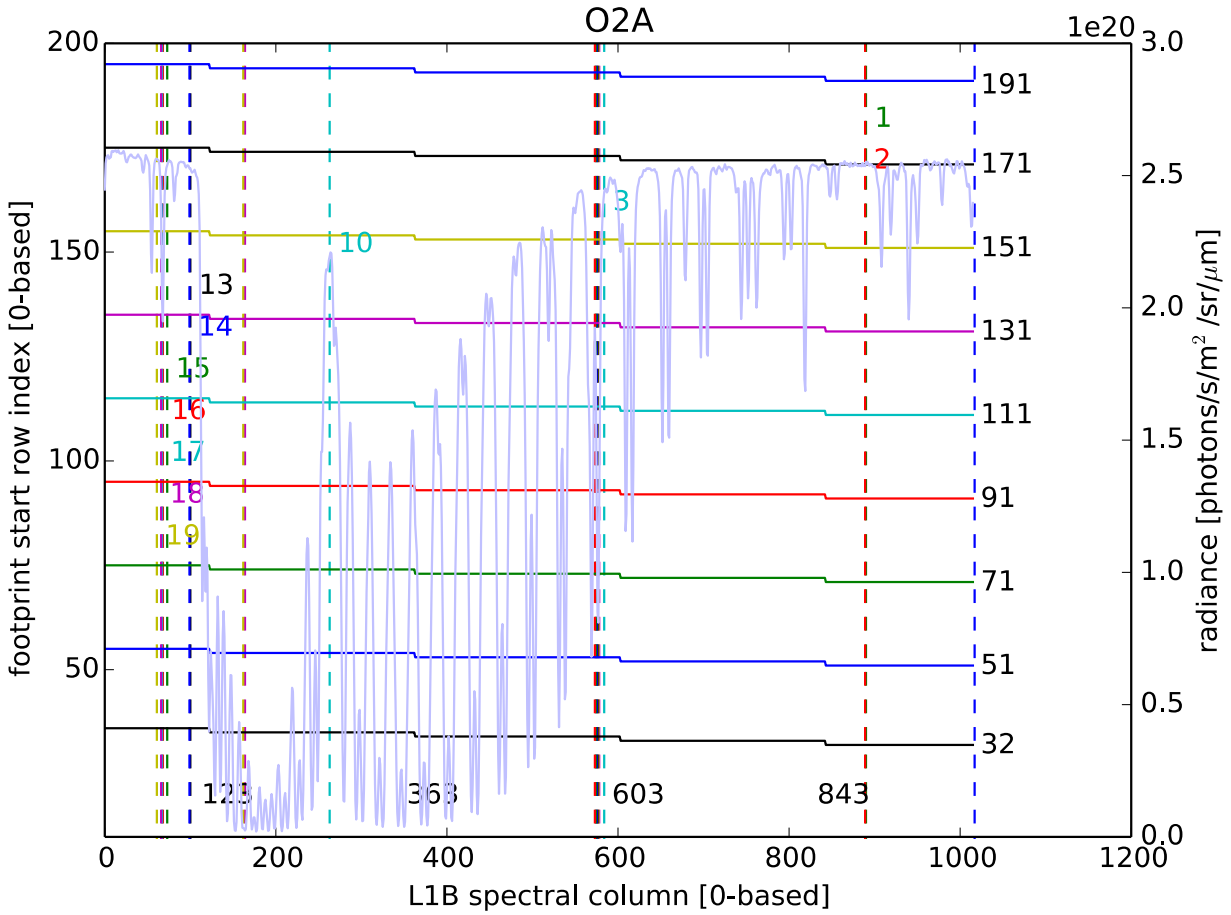

Figure 9: Schematic illustrating the clocking for the O2A band along with the current color slice selection. Piecewise-constant solid curves delineate footprint boundaries. Dashed vertical lines indicate color slice selection. Only those that are numbered are used for clocking. Finally, a typical spectrum of the band is overlaid for reference.

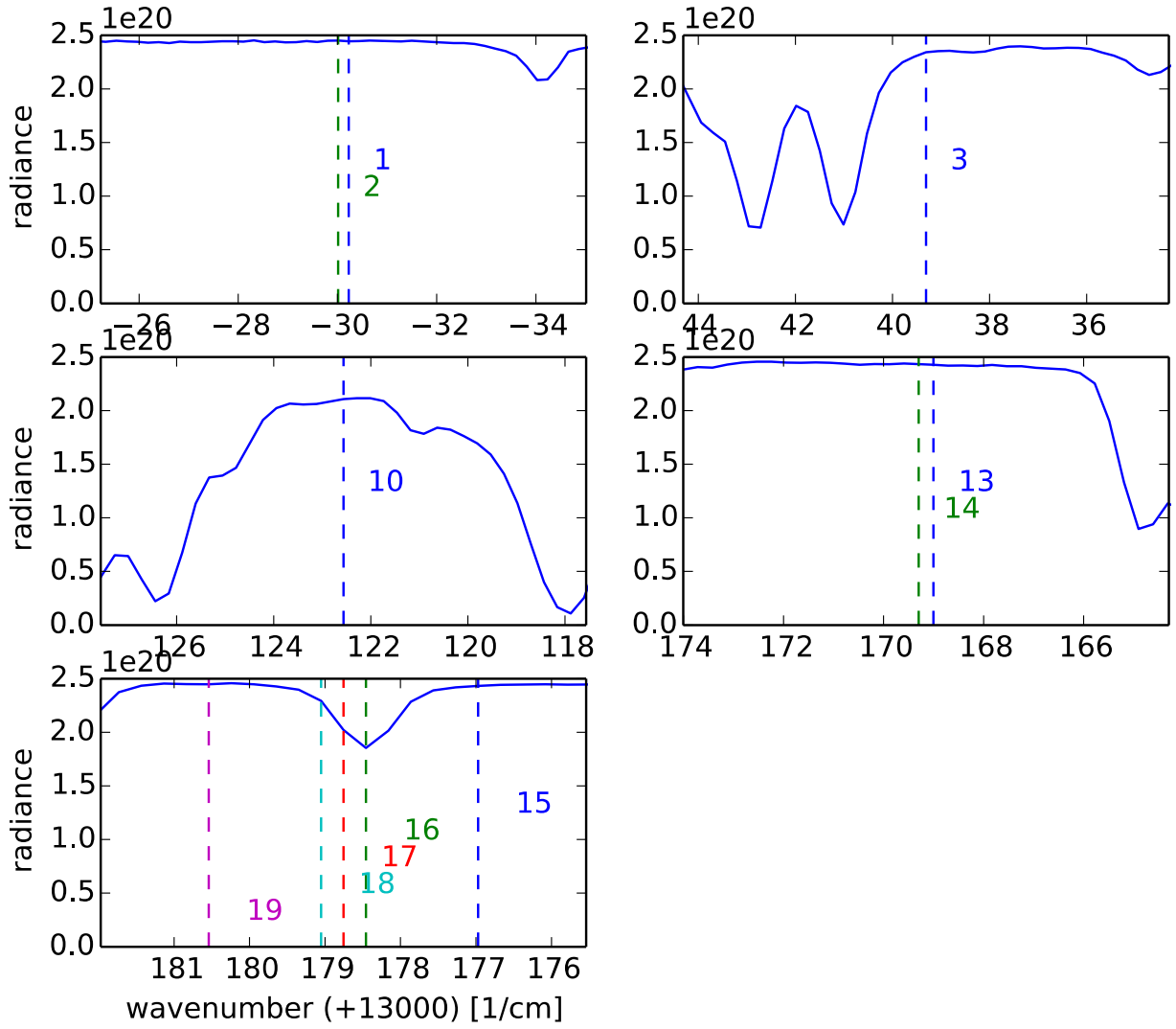

Figure 10: Close ups of selected color slices shown in Figure 9.

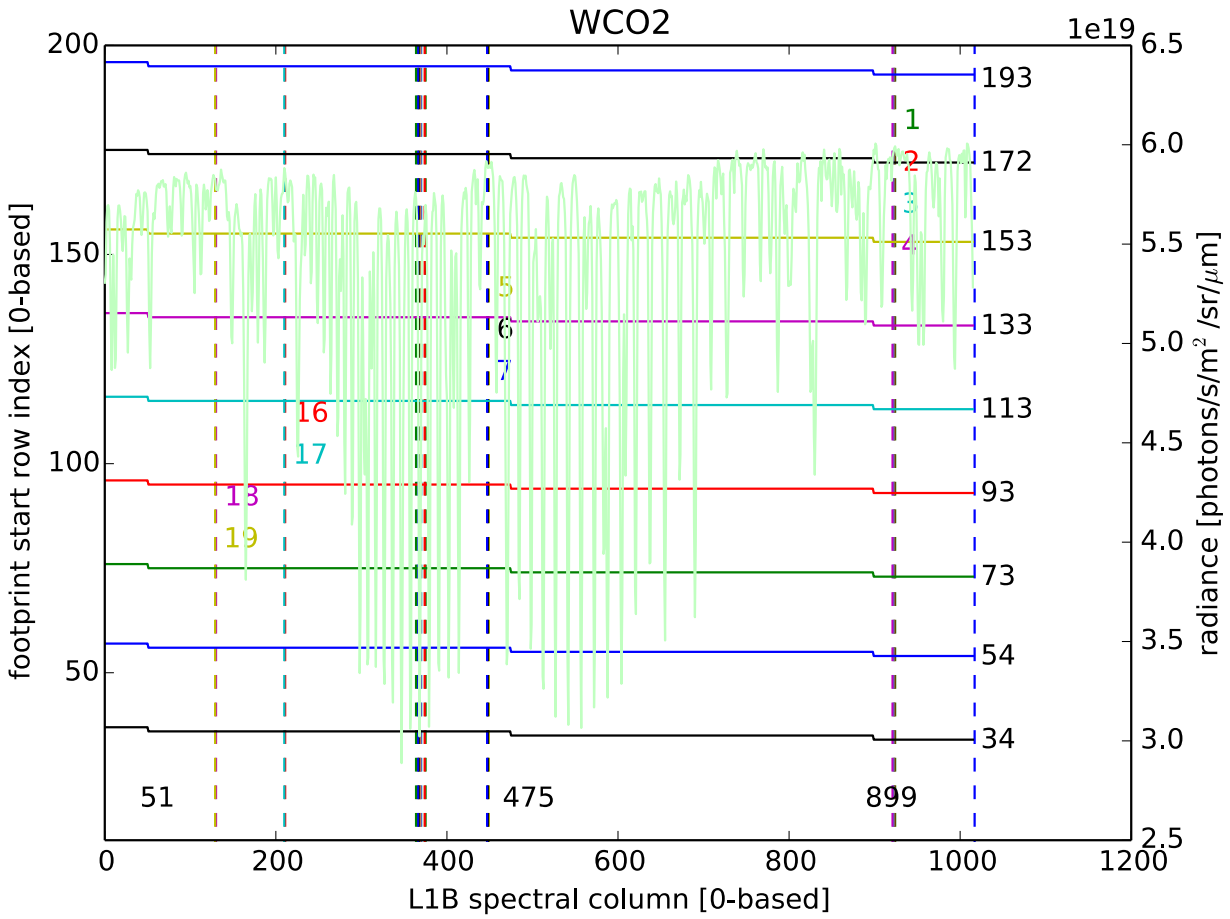

Figure 11: Schematic illustrating the clocking for the WCO2 band along with the current color slice selection. Piecewise-constant solid curves delineate footprint boundaries. Dashed vertical lines indicate color slice selection. Only those that are numbered are used for clocking. Finally, a typical spectrum of the band is overlaid for reference.

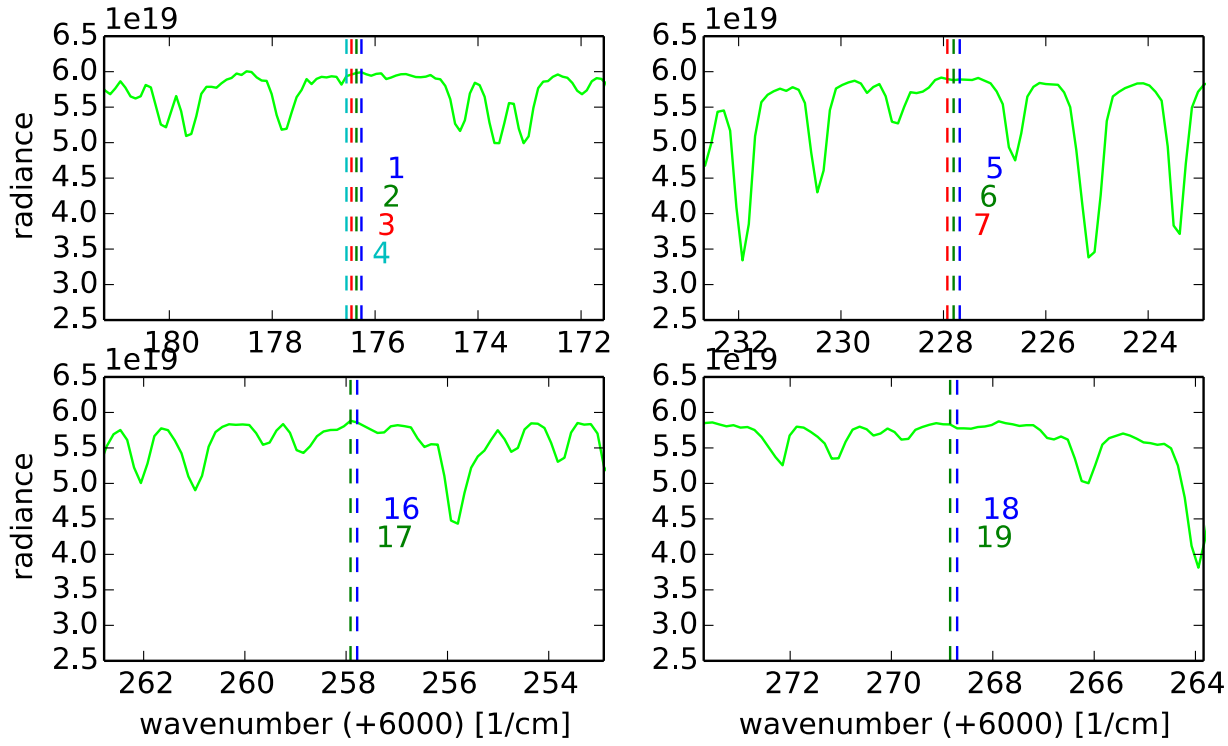

Figure 12: Close ups of selected color slices shown in Figure 11.

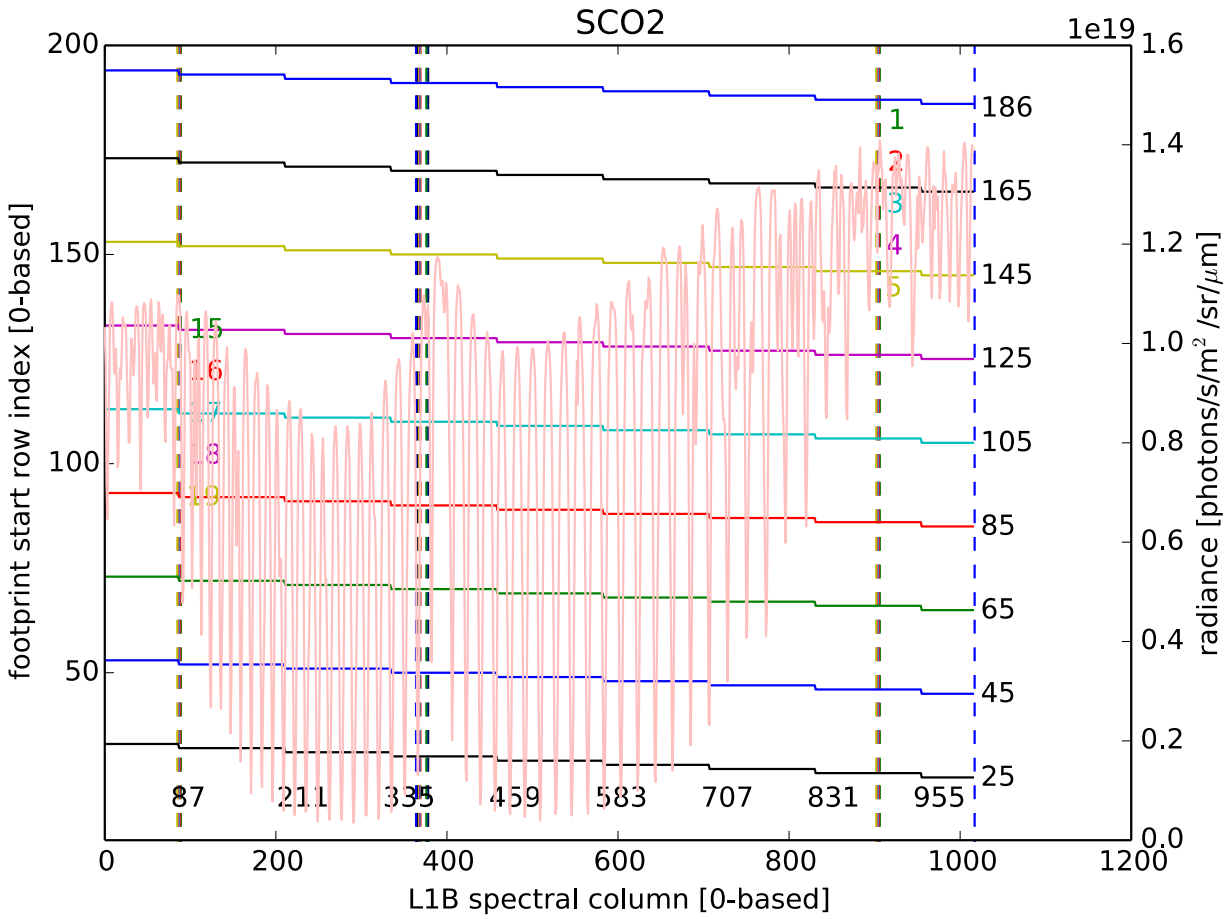

Figure 13: Schematic illustrating the clocking for the SCO2 band along with the current color slice selection. Piecewise-constant solid curves delineate footprint boundaries. Dashed vertical lines indicate color slice selection. Only those that are numbered are used for clocking. Finally, a typical spectrum of the band is overlaid for reference.

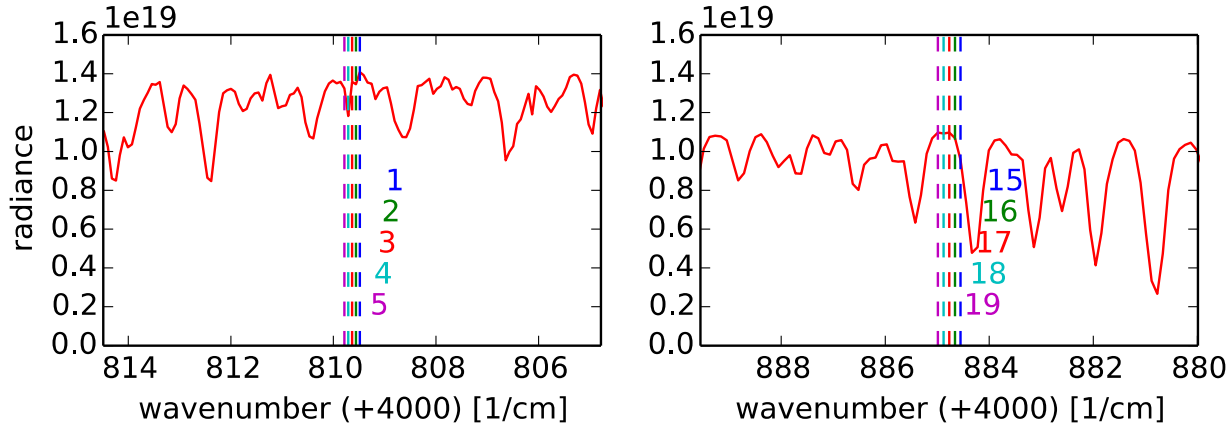

Figure 14: Close ups of selected color slices shown in Figure 13.

4.3.1 Clocking Algorithm Description

The algorithm used to compute modified L1B radiances proceeds in two stages. In the first stage, for each footprint-color slice pair, (*f,c*), average radiances over all possible footprint start and end positions are computed and saved to a file:

$$\bar{R}(f,c,j) = \frac{1}{M_{f,c}} \sum_{r \in FP(f)+j} R(r,c)$$

In this expression, *R(r,c)* is the radiance as a function of row *r* and color slice *c*, the sum is over all rows, *r,* contained in footprint, *f,* (as defined in the last column) but shifted by *j* pixels, and $M_{f,c}$ corresponds to the number of rows contained in the footprint-color slice pair.

Anomalous (e.g. negative) values must be eliminated so that they do not skew the averages, since they would lead to potentially large errors in the corrections. Therefore, a heuristic filtering is performed in which "bad" pixels are replaced with an average of nearest neighbors (in row space). Pixels are marked "bad" if they satisfy at least one of three conditions: (1) they are marked as "bad" in the ancillary radiometric product (ARP), (2) they have a negative value, or (3) the relative spatial gradient exceeds some threshold and the absolute spatial variation is more than twice the noise level σ, defined by

$$\sigma = \frac{R_{max}}{100}\sqrt{\frac{100R(\lambda)}{R_{max}}\eta_0^2 + \eta_1^2},$$

where $R(\lambda)$ is the radiance, R_{max} is an estimate of the maximum expected signal, and η_j are the signal to noise ratio (SNR) coefficients defined in the L1B file. The threshold is an adjustable parameter and taken to be a relative increase of 1.6 (or decrease of 1/1.6) from one row to the next. *The current scheme fails if there are two or more consecutive bad pixels.* This almost never happens for the O2A band, but does occur occasionally in the SCO2 band. Future implementations of the algorithm will take such pathological cases into account.

Figure 17 shows a large but not extreme example of the sort of spatial variation that might appear within a single frame. The grey, dotted vertical lines indicate footprint boundaries. Individual solid colored curves correspond to the *corrected* radiance within particular color slices, while all uncorrected radiance measurements are denoted by grey circles. Footprints 3 and 4 (counting from the left and starting from zero) show significant differences in both radiance and slope between their left and right boundaries. Such differences will produce large clocking corrections. Note also that there are three uncorrected points whose nearly vanishing values are replaced by averages of their neighbors. Without this correction the mean radiances within a footprint would be underestimated by ~5%. If the "bad" pixels occur near footprint boundaries and were to remain uncorrected, the clocking algorithm would produce erroneous corrections.

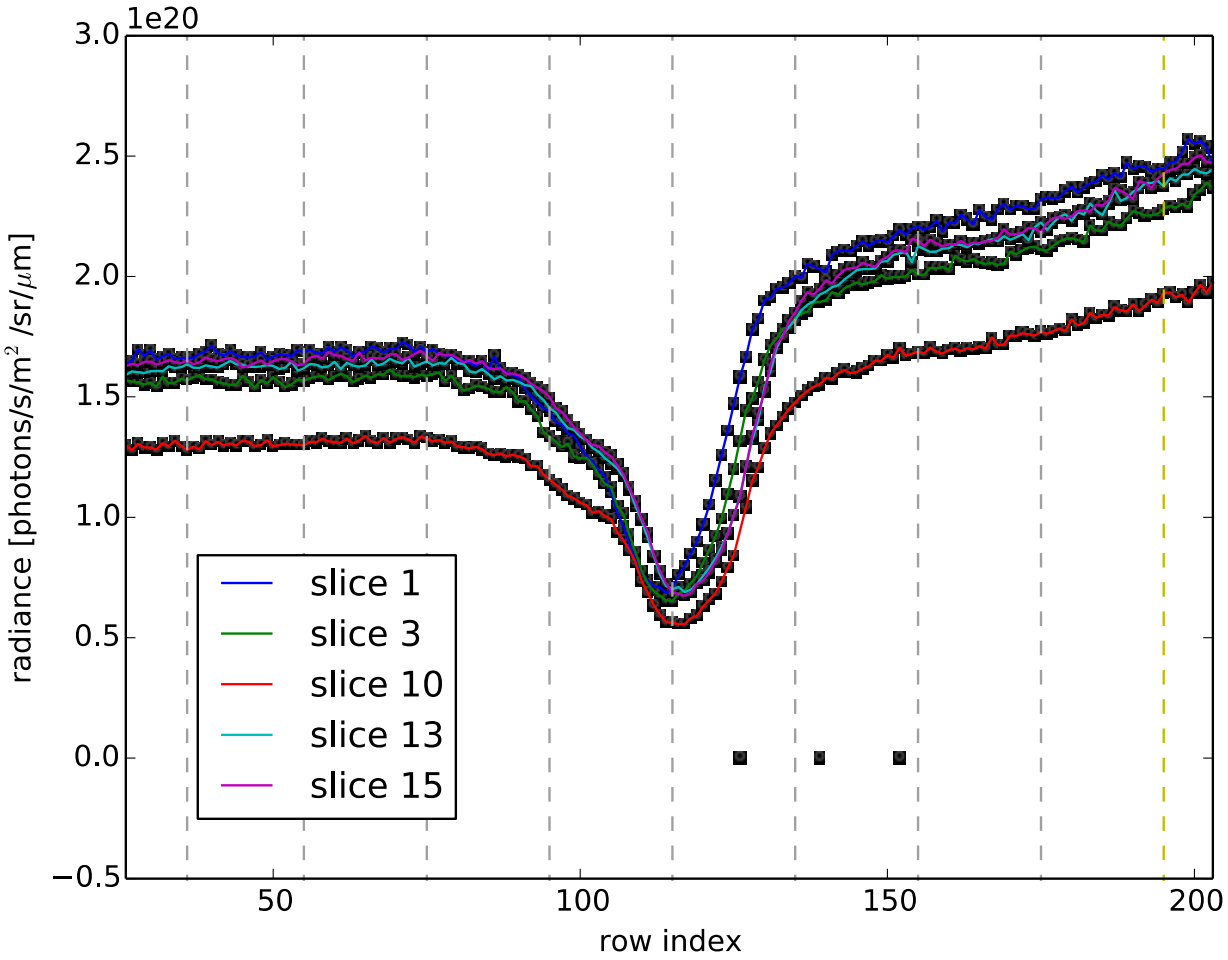

Figure 15: O2A band radiances measured for a few select color slices as a function of row index, which serves as a proxy for actual spatial variation within a scene. Solid curves are corrected values in which "bad" pixel data have been removed. Grey circles represent original measured data. For this particular case, three bad pixels have been replaced by nearest neighbor averages. Grey vertical lines represent footprint boundaries. The large differences between the values of the radiance on the boundaries of footprints 3 and 4 (starting from zero on the left) will produce large "clocking errors", or spectral discontinuities in the measurement.

After computing and saving the radiance means, the algorithm proceeds to the second stage in which column radiances are modified. First, the set of color slices is partitioned into "groups", which consist of clusters of spectrally close columns. The motivation for this partition is statistical. Using color slices that are spectrally very close should produce similar discontinuities; averaging over a small ensemble of strongly correlated slices reduces statistical error. The aggregation of color slices into groups follows a simple rule: two slices are in the same group if they are separated by fewer than n pixels, where n is taken to be 6 by default but is adjustable. (If n were chosen to be 0, for example, the groups would all be singletons.) In the future this rule may be further refined, possibly by allowing for aggregations that are dependent on footprint. Then, for each group, the ratio of the mean radiance at each jump is computed:

$$\mathrm{r(f,G,j)} = \frac{1}{N_{f,G}} \frac{\sum_{c\in G} \bar{R}(f,c,j)}{\sum_{c\in G} \bar{R}(f,c,j+1)}$$

In this expression the summation is over all color slices, c, within a group, G, and $N_{f,g}$ is a normalization factor defined below. (Of course, all radiance variables depend also on frame index, which has been omitted for notational clarity.) Neglecting the normalization factor for the moment, these ratios define multiplicative factors that if applied to one side of a jump, produce a continuous radiance across the jump. In many cases these ratios may be very close to unity. If for all jumps, the noise as defined above is greater than |r-1|/2, then the ratios are artificially set to one, so that no clocking correction is made.

Having calculated multiplicative factors needed to ensure continuity at jump locations, we now need to interpolate (and possibly extrapolate) to all spectral points. To achieve this, we linearly interpolate from a value of one from the first pixel beyond the previous jump to the ratio described above at the location of the current jump. The resulting correction function, $C_G(f,\lambda)$, is a sawtooth defined for each group G and at every spectral point λ. To maintain roughly the same average radiance across the entire band, this correction function is normalized such that its average over the entire spectral domain is equal to unity. The Figure 18 is an example of a correction function for the O2A band. On the left are raw correction functions for each group (in varying shades of blue) and for a particular frame and footprint but prior to renormalization. The corresponding functions after renormalization are plotted on the right in various shades of red.

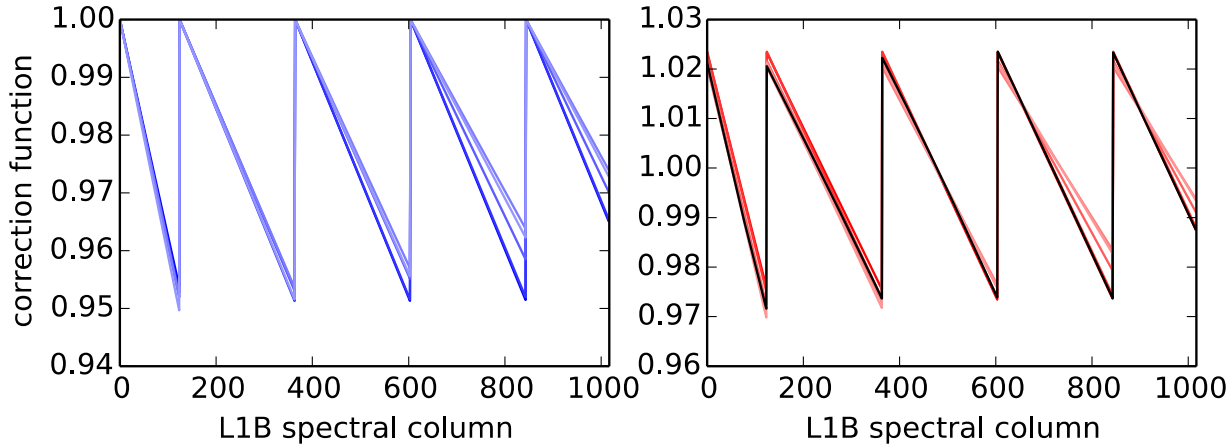

Figure 16: Example of a clocking correction function for the O2A band. The blue curves on the left correspond to different pre-normalized correction functions a determined by different groups of color slices for a single frame and footprint. To (roughly) preserve the value of the average radiance, the correction functions are normalized such that the mean over columns equals one, as shown in the red curves on the right. Multiplication by weighting functions for each group yields the final correction function, depicted as the black curve on the right.

At this point, one has multiplicative correction functions for each color slice grouping. These functions need to be combined to produce a single correction function, $C(f,\lambda)$, for each frame-footprint pair. Because the corrections are expected to be most accurate for columns that are spectrally close to a group, we employ simple hat functions to create a weighted average:

$$C(f,\lambda) = \sum_G h_G(\lambda) C_G(f,\lambda),$$

where $h_G(\lambda)$ are the triangular weighting functions, which fall linearly from a maximum value of one at the average column position of group G to a value of zero at the average positions of the neighbors of G. If G is the first or last group -- that is, it does not have a neighbor to the left or to the right – then $h_G(\lambda)$ has a constant value of one from the average column position to the end of the detector. Note that the hat functions depend only on the choice of color slices and their grouping and have the property that

$$\sum_G h_G(\lambda) = 1$$

The weighting functions for the current selection of color slices and groupings for the O2A band is shown in Figure 17, where each color corresponds to a different group, G:

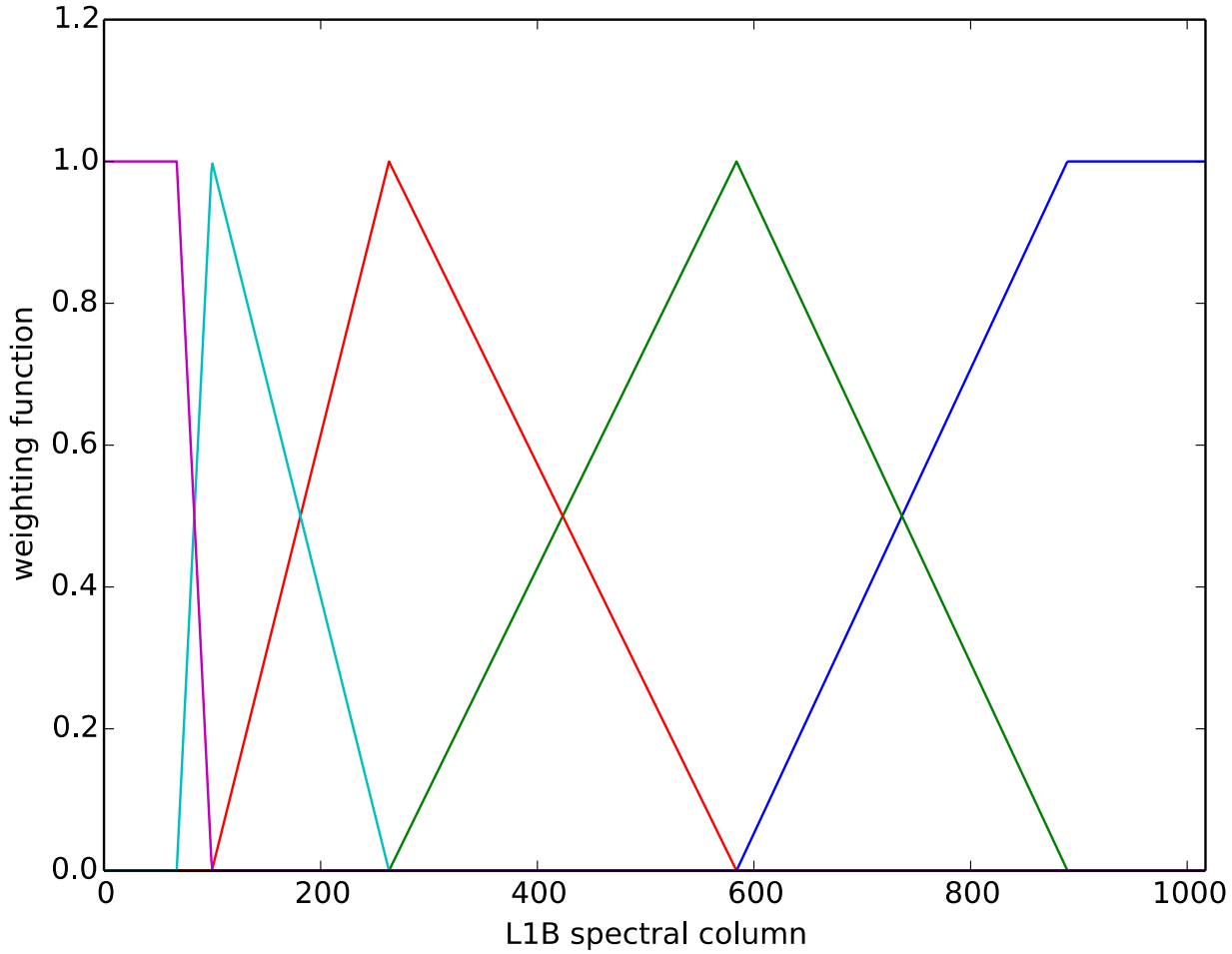

Figure 17: Weighting functions for each group of color slices for the O2A band.

The sum of the product of these weighting functions and the curves in red in Figure 18 yields the weighted average correction function, shown in black in Figure 18. This weighted correction is applied to the original L1B radiances to produce the corrected radiances:

$$R_{corrected}(f,\lambda) = R(f,\lambda) C(f,\lambda)$$

In practice most corrections for non-lunar scenes are fairly small; the difference between the original and corrected radiances is barely perceptible, although discontinuities may be more evident in the residuals of retrievals. A typical "large" correction is on the order of several percent. Figure 20 shows the effect of applying the correction illustrated in the preceding figures to the measured radiance of the O2A band. The black/red curves denote original/corrected radiances. Figure 11 shows that a clocking jump occurs at column 843. The inset illustrates the elimination of the discontinuity at that pixel to produce an even continuum region about the O_2 doublet.

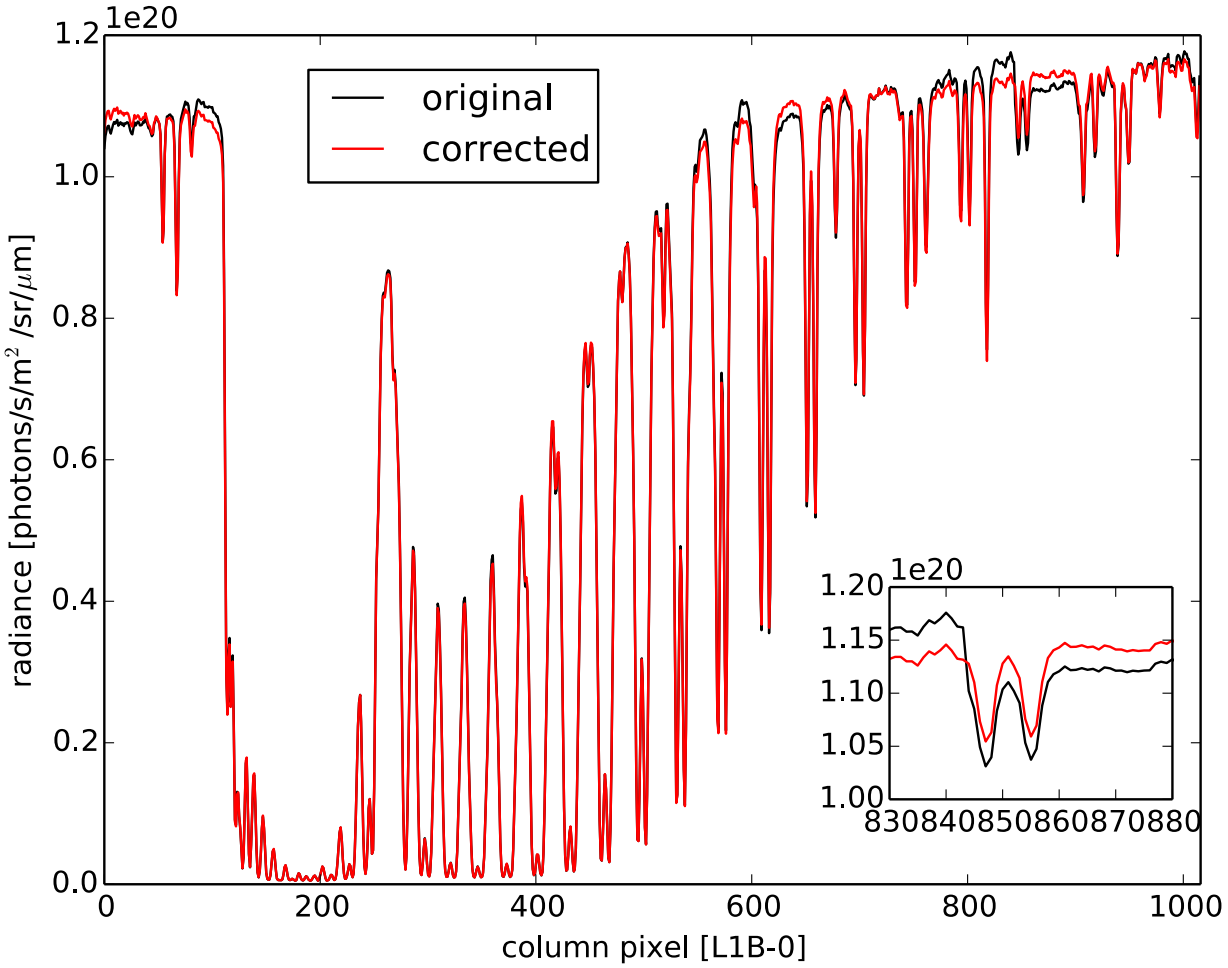

Figure 18: An example O2A spectrum, both before and after clocking correction. The inset shows a close up in the neighborhood of a jump, where the correction is largest.

4.3.2 Discussion

The behavior of the clocking correction varies significantly among the three bands. In this section, we restrict discussion to a comparison of the effect of the correction on a representative L1B product (orbit 1600); its impact on actual XCO2 retrievals will not be considered here. Orbit 1600, shown in

Figure 19 contains both land (33%) and ocean frames (66%).

We define a correction magnitude for a given frame-footprint pair to be the maximum over all 1016 spectral columns of the absolute value of the correction function minus one. It serves as a simple scalar metric by which to measure the size of the correction function for a given frame-footprint pair. Figure 20 shows the cumulative distribution of the magnitude of the correction for each band and terrain type (i.e. land and water). For example, for the O2A band roughly 90% of all frame-footprint pairs over land require a correction of less than 0.5%. While the statistics for the O2A and WCO2 bands are similar over land, the SCO2 bands requires larger corrections: the 90th percentile for the SCO2 occurs at a correction magnitude of 1%. The reason for this difference is unclear but may be related to the much larger number of "bad" pixels in the SCO2 band. We note that for each case shown in Figure 20 at least 40% of scenes require no correction at all. This result is an artifact of the noise cutoff threshold discussed in the previous section; corrections that are of the same order of magnitude as the noise are artificially set to zero.

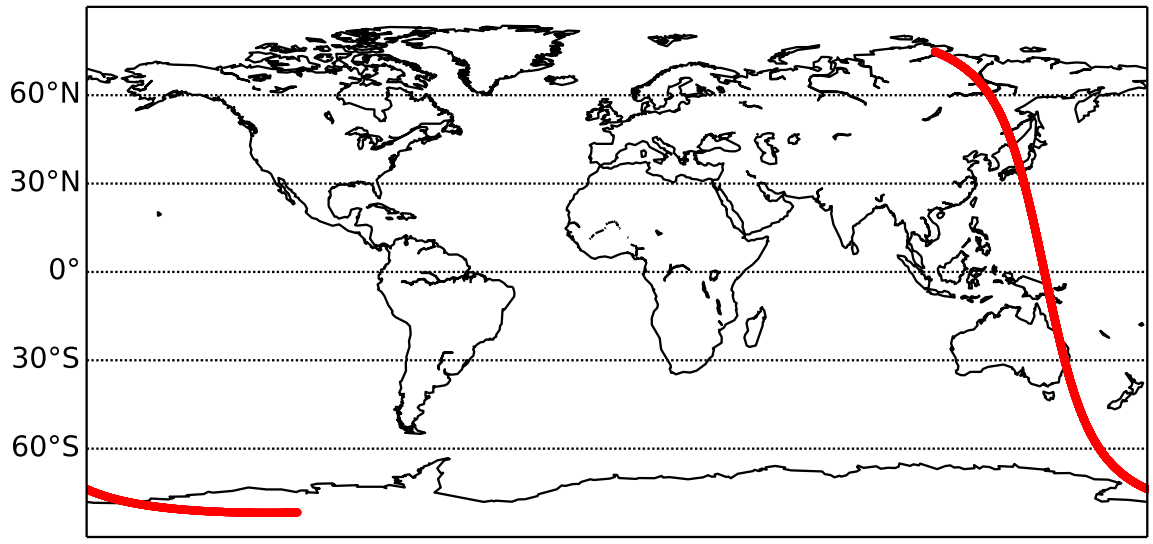

Figure 19 Orbit used in discussion of the clocking correction.

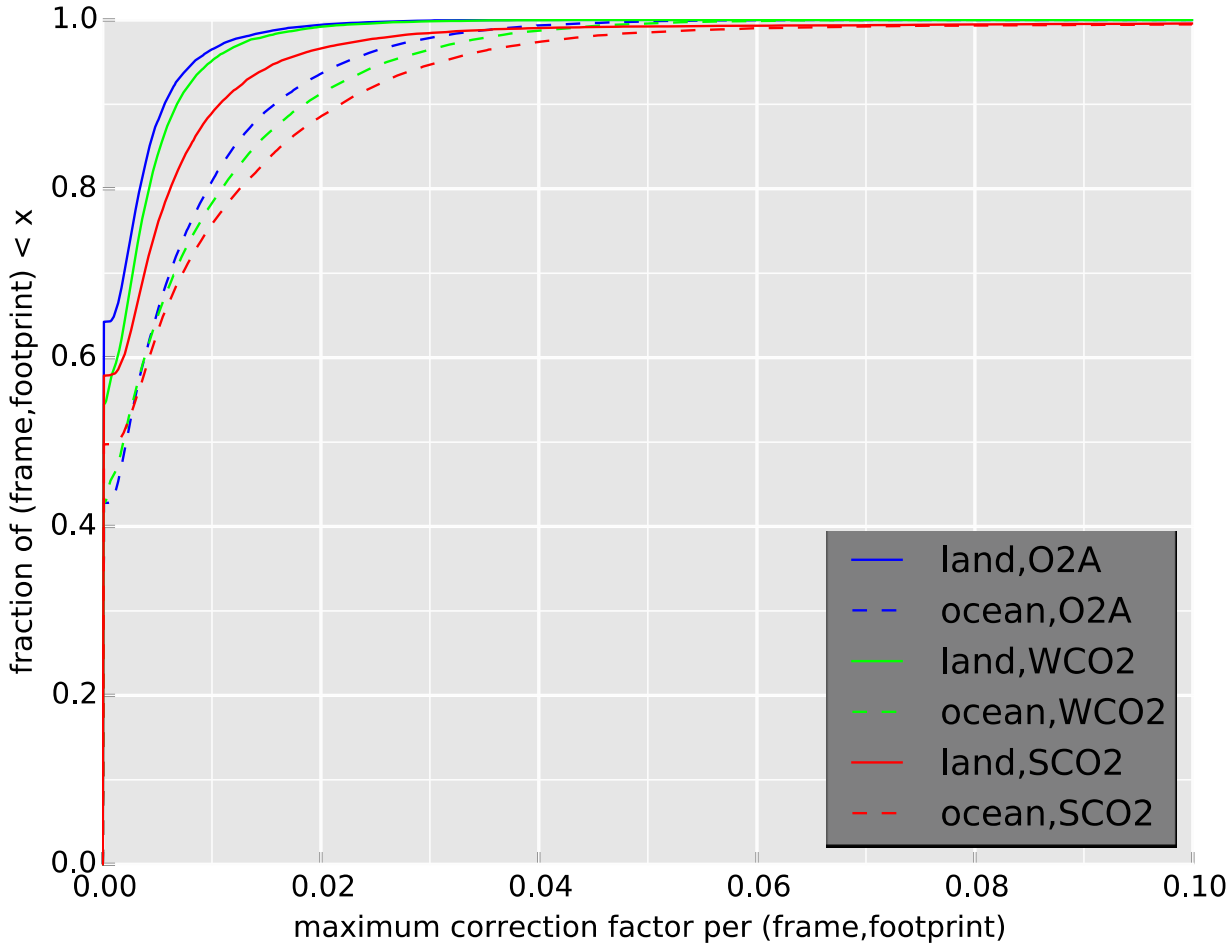

Figure 20: cumulative distribution function of magnitude of the correction for orbit 1600. Results are separated by band and terrain type (i.e land and water).

One useful metric to assess the soundness of the correction of the algorithm is to examine the consistency of the predicted corrections among the color slices. Figures 15, 16, and 17 show for the O2A, WCO2, and SCO2 bands, respectively, the correlation coefficient, ρ, of the ratios r, defined in the previous section:

$$\rho(f,G,G') = \frac{\sum_{s,j} r(s,f,G,j)r(s,f,G',j)}{\left(\sum_{s,j} r^2(s,f,G,j)\right)^{1/2}\left(\sum_{s,j} r^2(s,f,G,j)\right)^{1/2}},$$

where the summation over a frame index variable s has been made explicit and instead of the employing the grouping described previously, we've taken each group G to contain a single color slice. It was shown previously that a significant fraction of corrections are either small or identically zero. Since large relative differences of very small quantities may not be meaningful, we impose a restriction to the summation in the equation above: for a given group (i.e color slice) G we sum over only those corrections that are larger than a cutoff of 0.5%. Note that because the set of summands for a group G will not be identical to the set of summands for a group G', the correlation coefficient defined above will not generally be a symmetric function of G and G'.

Figure 21 shows the correlation matrix by footprint for the O2A band. We first note that the correlations are rather strong in all cases, everywhere exceeding 0.87. Also, as expected, color slices that are spectrally close have stronger correction correlations. This finding justifies our aggregation of color slices into groups. However, note that there is a dependence on footprint: spectrally distant color slices show greater consistency for lower footprint indices than for higher indices. That is, for higher footprint indices a more diverse sampling of color slices is required for the correction algorithm. This result is most apparent for the O2A band but is evident for the other bands as well. Finally, it was noted earlier that slices 16, 17, and 18 (corresponding to colors 68, 67, and 66) actually lie near solar lines and therefore ought not have been included in the correction algorithm. It was asserted that their inclusion, nonetheless, would not significantly modify the final outcome. The strong correlation illustrated in Figure 21 between those color slices and all the other slices on the shortwave end justifies that assertion.

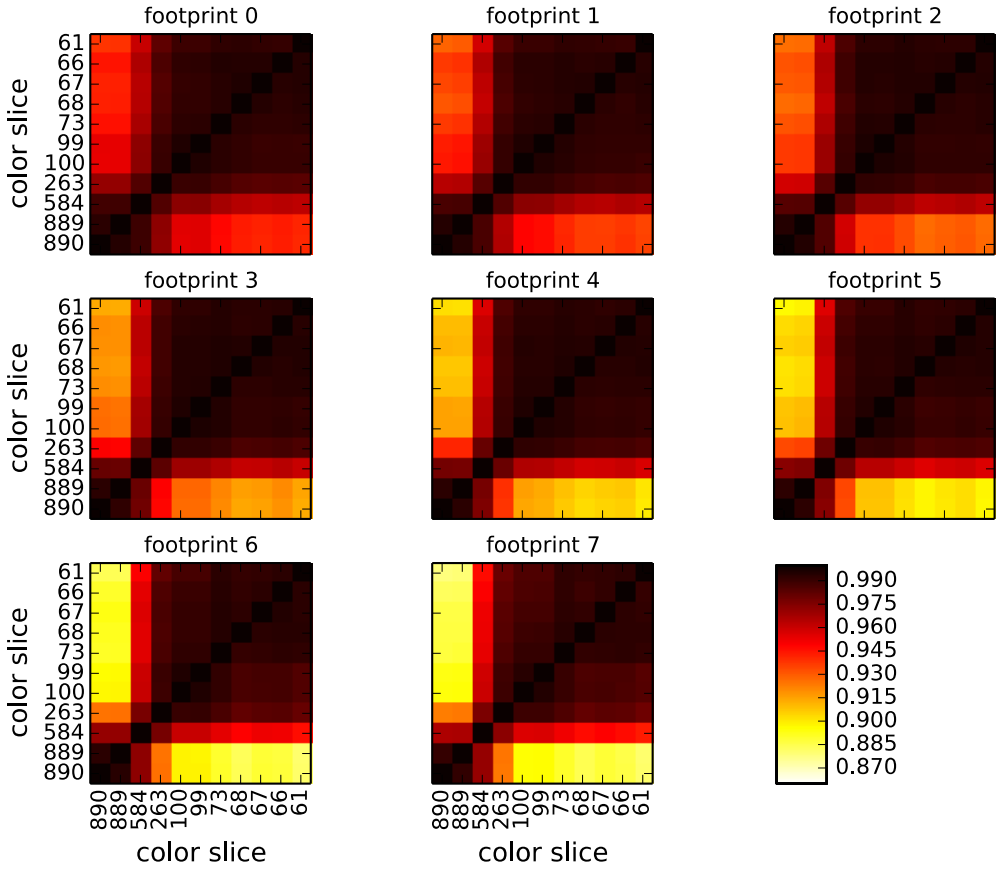

Figure 21: Correction correlation matrix for the O2A band.

Figure 22 shows correlations between color slices for the WCO2 band. Generally, the correlation matrix elements are even stronger than for the O2A band even for spectrally distant slices. This is likely due to the low degree of clocking in the WCO2 band, which suffers only three jumps over the whole band as compared to four in the O2A band and eight for the SCO2 band. However, there are some oddly weaker correlations involving color 211 in footprints 5

and 6 and color 922 in footprints 0 and 1. We suspect these arise from a greater number of instances where consecutive "bad" pixels foil the correction algorithm.

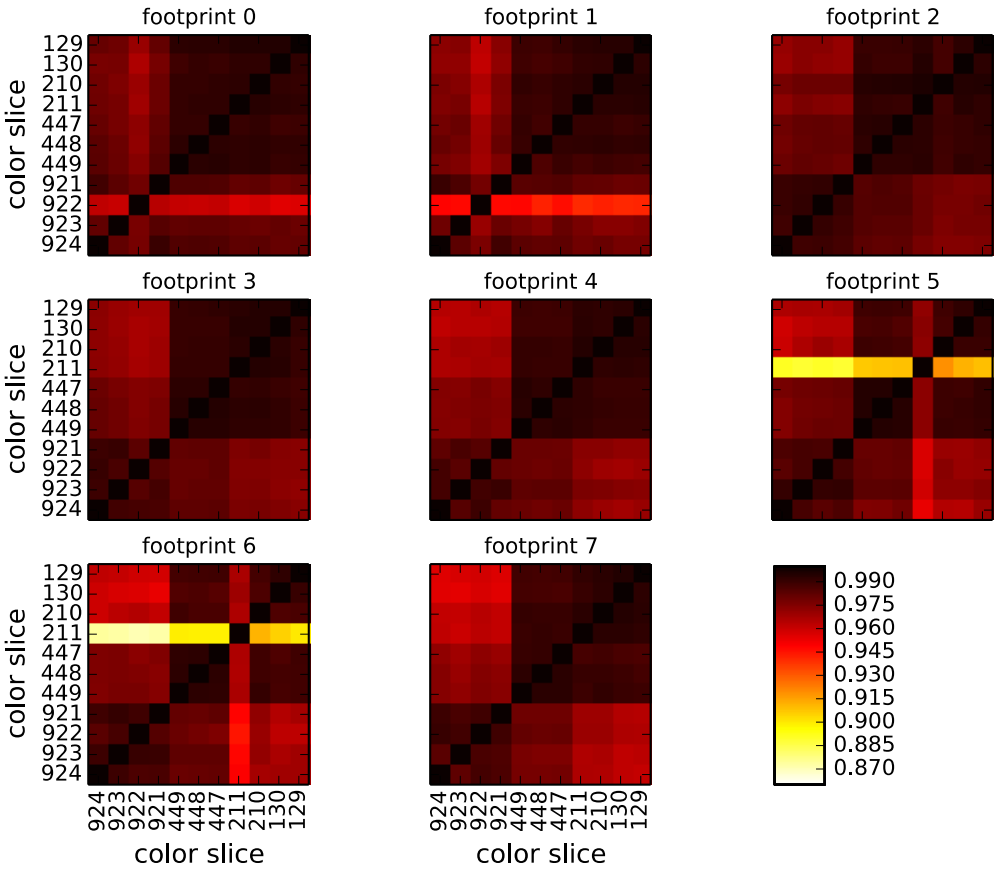

Figure 22: Correction correlation matrix for the WCO2 band

Unlike the other two bands, the corrections prescribed by color slices in the SCO2 band are not generally very consistent, even for spectrally nearby slices as Figure 23 shows. We strongly suspect that this result stems from the much larger number consecutive "bad" pixels, which the algorithm fails to properly handle. Note that the group of color slices 1-5 (colors 89 through 85) that do generally produce consistent corrections lie on the shortwave end of the detector, where there are far fewer pixels that are marked as "bad" in the ARP. Furthermore, the large clocking effect in the SCO2 should weaken the correlation between the two groups on the long and short wavelength ends of the detector.

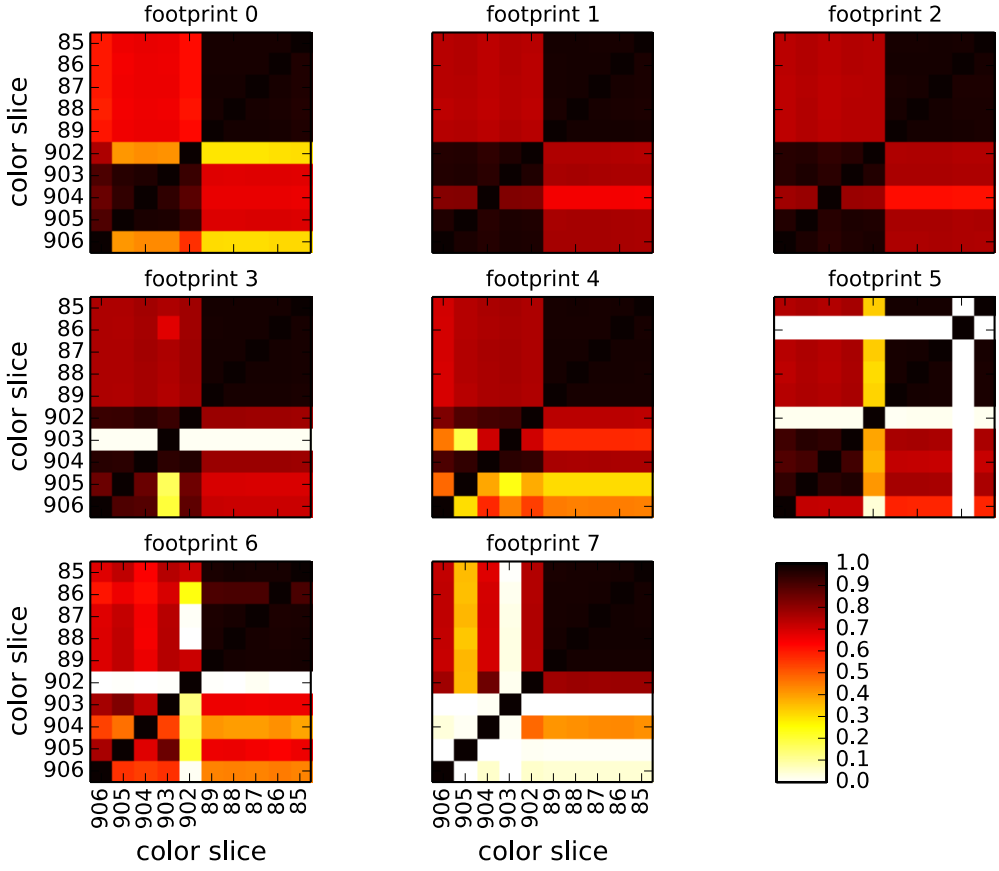

Figure 23: Correction correlation matrix for the SCO2 band

Finally, we consider the effect of the algorithm on the spectra themselves. One method to visualize the reduction of clocking-induced discontinuities is to perform a singular value decomposition on a set of spectra before and after correction and examine the resulting change in the right singular vectors:

$$S = U\Sigma V^*$$

In this expression the columns of S are comprised of the uncorrected spectra, Σ is the diagonal matrix of singular values, and the columns of U and V are the left and right singular vectors. Figure 24 demonstrates the effect of the clocking algorithm on the set of spectra in orbit 1600. The first eight singular vectors are plotted both before (top row) and after (bottom row) correction. Discontinuities that are clearly visible in the sixth (yellow-green), seventh (orange), and eighth (red) singular vectors prior to correction are completely eliminated by the clocking algorithm. Because only a minority of spectra require significant correction, the size of the effect as measured by the ratio of singular values is fairly small; the ratio of sixth and first singular value is 0.0045 in this data set. The impact of the correction on the other bands is similar and shown in figures 27 and 28.

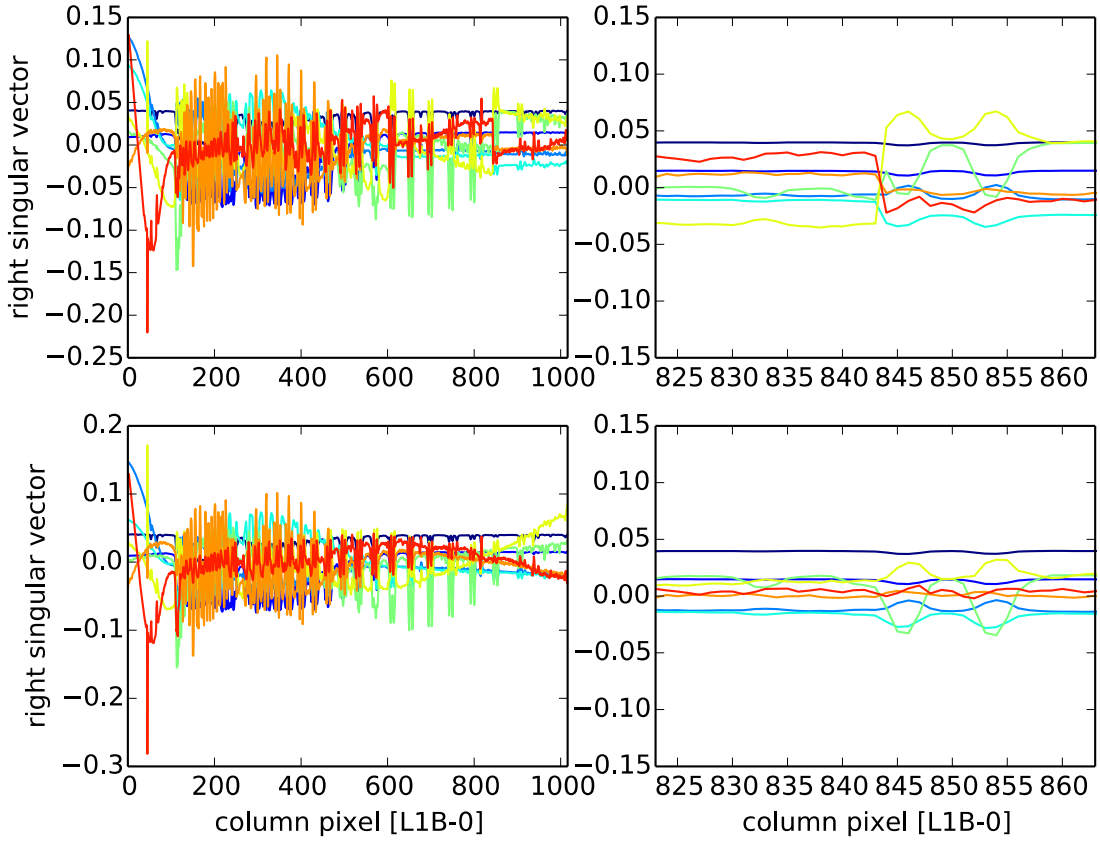

Figure 24: Right singular vectors corresponding to eight largest singular values from violet (largest) to red (smallest). The top /bottom rows are pre/post corrected vectors. The panels on the right are close up of clocking jumps at 843. The right singular vector corresponding to the sixth (yellow-green), seventh (orange), and eighth (red) largest singular values exhibit discontinuities at pixel 843 prior to correction.

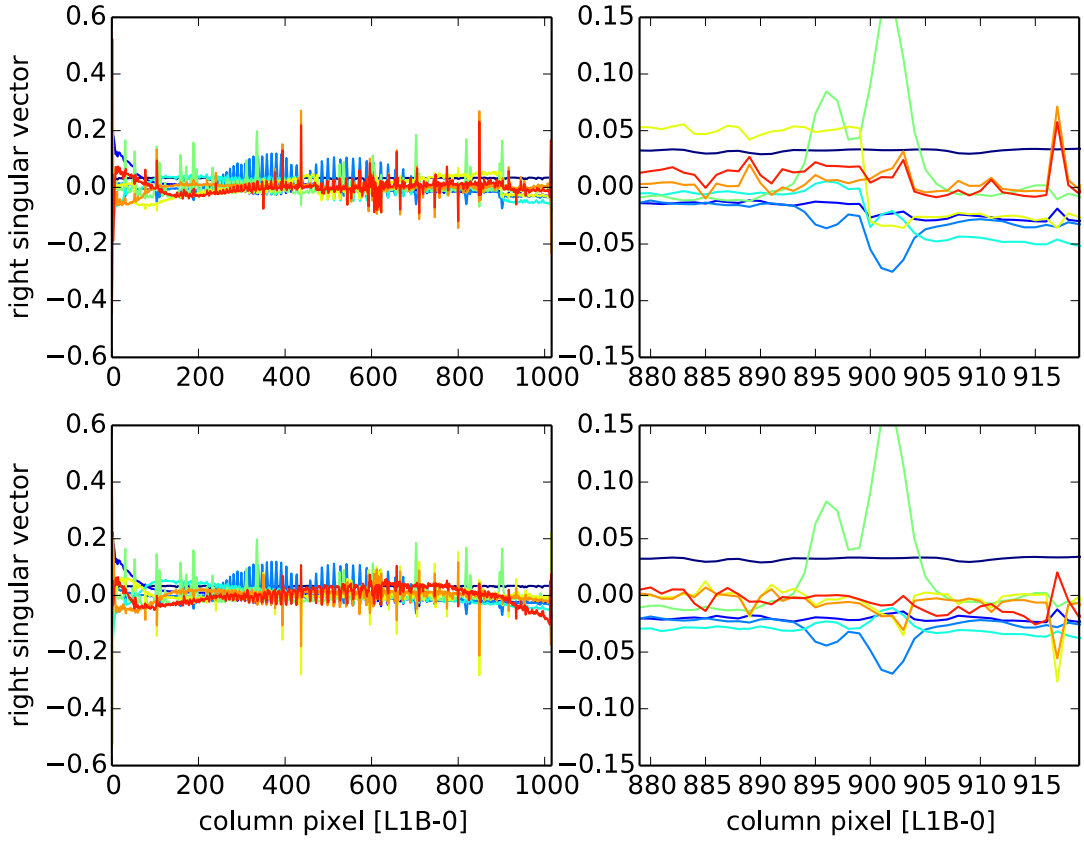

Figure 25: First eight right singular vectors for the WCO2 band. The clocking jump evident in the sixth one (in yellow-green) with singular value 0.28% of the largest value vanishes after the clocking correction.

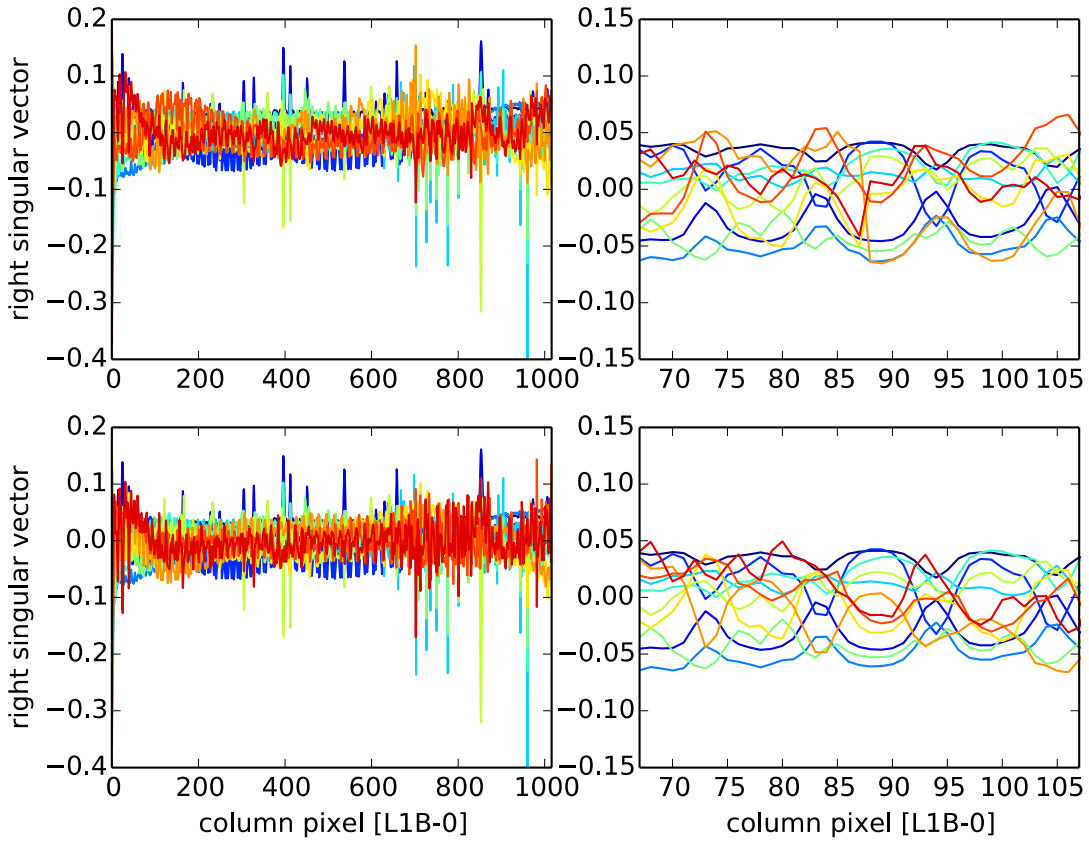

Figure 26: First twelve right singular vectors for the WCO2 band. The clocking jump evident in the eleventh one (in orange) with singular value 0.34% of the largest value vanishes after the clocking correction.

These results indicate that this correction approach will usually be adequate. In cases where it is not, it will produce a poor fit in the Level 2 retrieval, and the Level 2 post-processing screening algorithm will usually reject the sounding.

5. Ancillary Radiometric Product Files

The key calibration parameters are stored in the ARP, which is not distributed publically. These files are changed as needed and deemed necessary. There will be an ARP file for initial processing and an updated ARP for reprocessing to reflect any additional knowledge gained from the measured data set about temperature dependence, dark subtraction, etc. Each of the data products identifies the ARP used in Metadata/ARPAncillaryDatasetDescriptor.

6. Other Resources

There are a number of other project documents that the user should refer to as they work with the data.

1. Data User's Guide—This document discussed the publically distributed data products, L1bSc, L2IDP, L2Std, and L2Dia. The key data fields are discussed, and tables are included that specify all of the fields in each data product.
2. L2 ATBD—This ATBD steps through the physics and implementation of the Level 2 algorithm.
3. ATBD for IMAP-DOAS and ABO2—These ATBDs describe the two methods of identifying potentially cloudy footprints, in what we refer to as the prescreening step. These data are then used for setting data quality and data selection levels.
4. Published papers—There are a number of published papers describing the algorithm, application to GOSAT, prescreening steps, etc. Please see the most up-to-date list of publications on oco2.jpl.nasa.gov

7. References

Crisp, D., C. E. Miller, and P. L. DeCola, NASA Orbiting Carbon Observatory: Measuring the column averaged carbon dioxide mole fraction from space, *JARS*, (2007).

Crisp, D., The Orbiting Carbon Observatory: NASA's First Dedicated Carbon Dioxide Mission, *Proc. SPIE,* 7106 (2008). doi: 10.1117/12.802194.

Kuze, Akihiko, et al. Long-Term Vicarious Calibration of GOSAT Short-Wave Sensors: Techniques for Error Reduction and New Estimates of Radiometric Degradation Factors. *IEEE Transactions on Geoscience and Remote Sensing,* 52.7 (2013): 1-14.

Kuze, Akihiko, et al. Vicarious calibration of the GOSAT sensors using the Railroad Valley desert playa. *IEEE Transactions on Geoscience and Remote Sensing*, 49.5 (2011): 1781-1795.

Lee et al., Preflight Spectral Calibration of the Orbiting Carbon Observatory-2, in preparation, 2015.

O'Dell, C. W., J. O. Day, R. Pollock, C. J. Bruegge, D. M. O'Brien, R. Castano, I. Tkatcheva, C. E. Miller, and D. Crisp, Preflight Radiometric Calibration of the Orbiting Carbon Observatory *IEEE Transactions on Geoscience and Remote Sensing*, 49.6 (2011): 2438-2447. doi: http://dx.doi.org/10.1109/TGRS.2010.2090887.

Rosenberg et al., Preflight Radiometric Calibration of Orbiting Carbon Observatory 2, in preparation, 2015.

Yoshida, Y., N. Kikuchi, and T. Yokota. On-orbit radiometric calibration of SWIR bands of TANSO-FTS onboard GOSAT. *Atmospheric Measurement Techniques Discussions*, 5.4 (2012): 4711-4734.